

MASARYKOVA UNIVERZITA
PŘÍRODOVĚDECKÁ FAKULTA
ÚSTAV TEORETICKÉ FYZIKY A ASTROFYZIKY

Diplomová práce

BRNO 2019

PETR KOBRLE

M A S A R Y K O V A
U N I V E R Z I T A
PŘÍRODOVĚDECKÁ FAKULTA
ÚSTAV TEORETICKÉ FYZIKY A ASTROFYZIKY

Pozorování a analýza optických protějšků záblesků gama

Diplomová práce

Petr Kobrle

Vedoucí práce: Mgr. Filip Münz, Ph.D. Brno 2019

Bibliografický záznam

Autor: Bc. Petr Koblre
Přírodovědecká fakulta, Masarykova univerzita
Ústav Teoretické fyziky a Astrofyziky

Název práce: Pozorování a analýza optických protějšků záblesků gama

Studijní program: Fyzika

Studijní obor: Teoretická fyzika a astrofyzika

Vedoucí práce: Mgr. Filip Münz, Ph.D.

Akademický rok: 2018/2019

Počet stran: ix + 61

Klíčová slova: gama záblesky, XRT, D50, redukce snímků, skládání snímku, dosvit, světelné křivky

Bibliographic Entry

Author: Bc. Petr Koblre
Faculty of Science, Masaryk University
Department of Theoretical physics and Astrophysics

Title of Thesis: Observation and analysis of GRB optical counterparts

Degree Programme: Physics

Field of Study: Theoretical physic and astrophysics

Supervisor: Mgr. Filip Münz, Ph.D.

Academic Year: 2018/2019

Number of Pages: ix + 61

Keywords: gamma-ray burst, XRT, D50, image data reduction, stacking, afterglow, lightcurve

Abstrakt

V této diplomové práci se věnujeme zdrojům zábleskového záření gamma (GRB) – konkrétně jejich protějškům v optickém oboru spektra. Jádrem práce bylo vytvoření kódu, pomocí kterého lze kompletně zpracovat optická pozorování, s jehož využitím jsme zpracovali dosvit konkrétního GRB. V první části se věnujeme krátkému úvodu k historii a důležitým milníkům ve výzkumu GRB. V druhé prezentujeme zatím nejúspěšnější model pro tento fenomén. Ve třetí části se věnujeme síti GCN, dalekohledu D50 a tématům souvisejícím s CCD astronomií. Ve čtvrté části popisujeme užívání balíku GRBLC společně s vysvětlením některých procedur a algoritmů. V poslední části uvádíme data a rozbor světelné křivky pro GRB 131030A v optickém a rentgenovém oboru spektra.

Abstract

This thesis is dedicated to study Gamma-ray bursts – specifically their optical counterparts. Core of this thesis was to create a code which can completely process optical observations, with which we analysed afterglow of a specific GRB. In the first part we briefly describe history and important milestones in GRB research. In the second part we present the most successful model for GRBs so far. The third part is dedicated to GCN network, D50 telescope and topics related to CCD astronomy. In the fourth part we describe usage of GRBLC package along with explaining some of its procedures and algorithms. In the last – fifth – part we present data for GRB 131030A along with our analysis of optical and X-ray afterglow light curve for this GRB.



ZADÁNÍ DIPLOMOVÉ PRÁCE

Akademický rok: 2017/2018

Ústav:

Student: Bc. Petr Koblře

Program: Fyzika

Obor: Teoretická fyzika a astrofyzika

Směr: Astrofyzika

Ředitel ústavu PíF MU Vám ve smyslu Studijního a zkušebního řádu MU určuje diplomovou práci s názvem:

Název práce: Pozorování a analýza optických protějšků záblesků gama

Název práce anglicky: Observation and analysis of GRB optical counterparts

Oficiální zadání:

Gama záblesky jsou fascinujícím projevem velmi energetických procesů v kosmologických vzdálenostech. Pozorují se v oboru gama záření a rentgenu z oběžné dráhy, a pomocí optických a radiových teleskopů z povrchu země. Cílem diplomové práce je přispět k pozorování optických dosvitů záblesků gama pomocí robotických dalekohledů a především zpracovat multispektrální pozorování takového gama záblesku, tedy zpracovat a jednotně interpretovat data získaná v gama záření, v rentgenu a v optickém oboru. Předpokládané činnosti: 1. Zapojit se do pozorování robotickým dalekohledem D50 Astronomického ústavu AV ČR, zvládnout redukci CCD snímků. 2. Zpracovat multispektrální světelnou křivku záblesku s významným pokrytím v optickém i rentgenovém oboru (např. GRB 131030A) 3. Vyvodit možné fyzikální závěry ohledně patřičných relací mezi spektroskopickými a fotometrickými vlastnostmi (Amatiho, Ghirlandův vztah), celkového výkonu a rychlosti vyvrhované hmoty apod.

Literatura:

LONGAIR, M. S. *High energy astrophysics*. 2nd ed. Cambridge: Cambridge University Press, 1992. xvii, 418. ISBN 0521387736.

Jazyk závěrečné práce: angličtina

Vedoucí práce: Mgr. Filip Münz, PhD.

Datum zadání práce: 16. 12. 2016

V Brně dne: 14. 2. 2017

Souhlasím se zadáním (podpis, datum):

.....
Bc. Petr Koblře
student

.....
Mgr. Filip Münz, PhD.
vedoucí práce

.....
ředitel ústavu

Poděkování

Na tomto místě bych chtěl poděkovat poděkovat svému vedoucímu Mgr. Filipu Münzovi, Ph.D. za vedení mé práce, cenné poznámky, rady a výpomoc s testováním GRBLC, a Mgr. Martinu Jelínkovi, Ph.D. za rady k textu a spolupráci. A též všem blízkým v mém okolí, kteří se mnou v době vzniku této práce dokázali vydržet. Howgh.

Prohlášení

Prohlašuji, že jsem svoji diplomovou práci vypracoval samostatně s využitím informačních zdrojů, které jsou v práci citovány.

Brno 13. května 2019

.....
Petr Koblre

Contents

Abbreviations	ix
Introduction	1
Chapter 1. Gamma-Ray Bursts	2
1.1 Brief history	2
1.1.1 Discovery	2
1.1.2 CGRO and BATSE experiment	2
1.1.3 Swift	6
Chapter 2. A little bit of theory behind GRBs	9
2.1 Fireball model	9
2.2 Amati and Ghirlanda relation	11
2.2.1 Amati relation	11
2.2.2 Ghirlanda relation	14
2.3 Long and Short Gamma-ray Bursts origins	15
2.3.1 Long GRBs and SN connection	15
2.3.2 Short GRBs	17
Chapter 3. Optical observations	19
3.1 GCN/TAN	19
3.1.1 GCN Notices	19
3.1.2 GCN Circulars	20
3.2 D50	21
3.3 Ground based optical observations	23
3.3.1 CCD Image reduction	23
3.3.2 Airmass	24
Chapter 4. GRBLC	26
4.1 Installation	26
4.2 Structure	26
4.2.1 Objects	27
4.2.2 Data handling	28
4.2.3 Operating with CCD data	32
4.2.4 Photometry	34

4.2.5 ShiftTransform	35
4.2.6 Image stacking	36
4.3 Procedure descriptions and algorithms	37
4.3.1 DarkTransform and FlatTransform	37
4.3.2 ShiftTransform	38
4.3.3 Photometry and Stacking	38
Chapter 5. GRB 131030A	42
5.1 GCN information	42
5.2 XRT data	45
5.3 D50 Optical data	47
Summary	53
Appendix	55

List of Used Abbreviations

BAT	Burst Alert Telescope
BATSE	Burst and Transient Source Experiment
BH	Black Hole
CGRO	Compton Gamma-Ray Observatory
GBM	Gamma-ray Burst Monitor
GCN	GRB Coordinates Network
GRB	Gamma-Ray Burst
GRBM	Gamma-Ray Burst Monitor
GW	Gravitational wave
HETE	High Energy Transient Explorer
INTEGRAL	INTErnational Gamma-Ray Astrophysics Laboratory
IPN	Inter-Planetary Network
LGRB	Long Gamma-Ray Burst
LIGO	Laser Interferometer Gravitational wave Observatory
NS	Neutron Star
SGRB	Short Gamma-Ray Burst
SN	Supernova
UVOT	UltraViolet/Optical Telescope
WD	White Dwarf
XRT	X-Ray Telescope

Introduction

This thesis is dedicated to Universe's most energetic explosions – Gamma-ray bursts. The theory behind it is still far from being complete, but some description and significant progress was made since their discovery almost fifty years ago. We focus on studying this phenomenon in its more inconspicuous form, observed with telescopes from ground, where unlike its blinding form in the gamma-ray sky, we could so far see only one with our bare eyes. Nowadays astronomy goes in a direction of automation, making systems and telescopes that can do all the work without a human interaction. It enables us to catch more and more of these transient events ever moment and allows us to study them, but the amount of data we collect is immense.

This thesis tries to tackle with the problem of processing data of optical observations produced by robotic telescopes, in a way that helps process them faster and more comfortable and allows us to focus more on the “why” than on routinely processing raw data again and again.

In the first chapter of this thesis we try to tell the tale of discovery of Gamma-ray bursts and name a few important milestones in Gamma-ray burst research. In second chapter we focus briefly on the known model for Gamma-ray bursts, present some of the known correlations, Gamma-ray Burst progenitors and discuss some of the latest news. In third chapter we present the system that provided us with optical observation data. The telescope used to acquire them and some points about CCD astronomy we have to deal with here on Earth. In fourth chapter we present a software/package that was we developed with aim of easier data processing and creation of optical light curves from automated observations. We thoroughly describe usage and explain some of the used algorithms. In the last, fifth chapter we present our analysis of GRB 131030A with data coverage in X-ray and optical bands.

Chapter 1

Gamma-Ray Bursts

Gamma-ray bursts as high energy phenomenon represent a fascinating display of nature's power. In this chapter we describe how we came to know a thing called GRB. We present some ideas how the engine behind it works and some physics behind why we think we see what we see is in chapter 2.

1.1 Brief history

1.1.1 Discovery

Discovery of Gamma-ray burst was, as many discoveries of other phenomena, accidental. It happened in 1967, when military satellites Vela of the US Department of Defense, designed to control fulfilling the Partial Test Ban Treaty (treaty forbidding testing of nuclear weapons between US, UK and USSR) detected a gamma-ray sources that were coming from space instead of ground. Data from satellites that detected gamma-rays coming from outer space were classified but shortly after declassification a first article about gamma-ray bursts was published [26] where sixteen detections of gamma-ray bursts from different Vela satellites were identified. In the following year these observations were confirmed with observations made by Russian satellite Cosmos-461 (Mazets et. al 1974).

1.1.2 CGRO and BATSE experiment

BATSE (Burst And Transient Source Experiment) on board of CGRO (Compton Gamma-Ray Observatory)[16] mission was an important milestone in gamma-ray burst research. This mission had total of four experiments covering broad detectable energy ranges (30 keV to 30 GeV). BATSE detected 2704 gamma-ray burst during its 9 year mission. This mission discovered two major properties – isotropic and bimodal distribution.

Isotropic and Bimodal distribution

BATSE experiment had poor spatial resolution but from all detected sources isotropic distribution could be confirmed nonetheless (see figure 1.2).

Figure 1.1: Detection of GRB 700822 from [26]. Arrows indicate identical features confirming that this is the same GRB detected on three different Vela satellites (5A, 6A and 6B). Vela 5A counts were reduced by about 100 count rates per second to emphasise the structure.

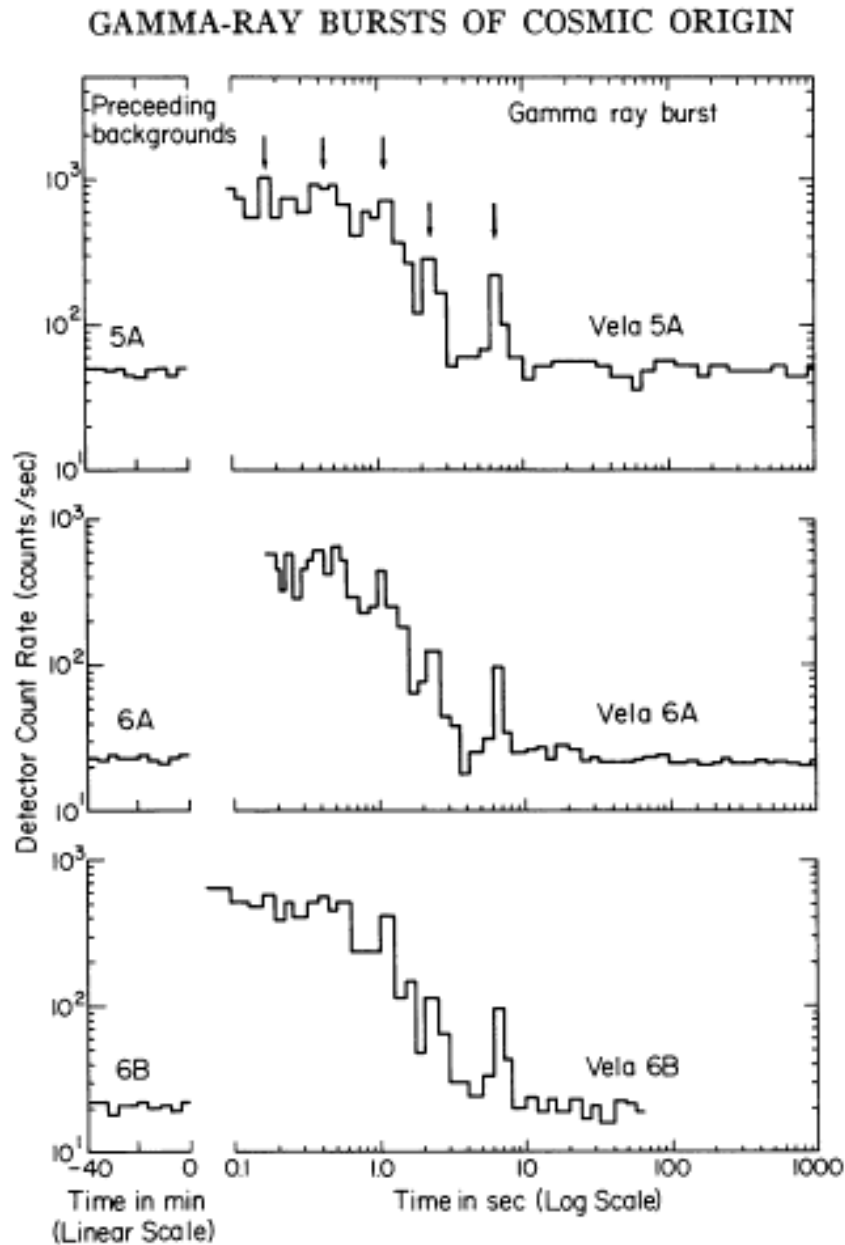
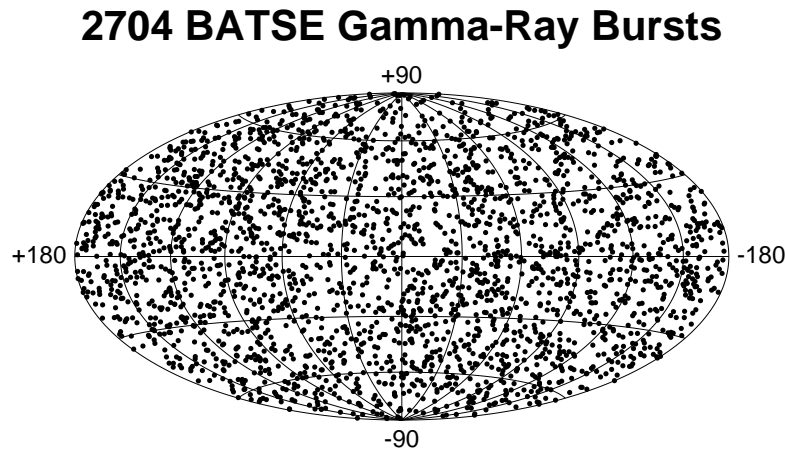


Figure 1.2: Image of GRB locations as detected by BATSE over its lifespan.



However, later studies, very detailed being [45], investigating isotropic distribution of BATSE sample, divided it into two long, two short and one intermediate group to test it for full randomness. The conclusion was that short and intermediate samples deviate significantly from full randomness in squared Euclidean distance (99.9 % to 99.98 % and 98.51 %, respectively). The long GRB groups did not deviate significantly.

Another important discovery was bimodal distribution which distinguishes two major groups of Gamma-ray bursts. The initial sample for analysis was the first BATSE catalog that consisted of 260 GRBs. The length of GRBs is measured so that for statistical robustness T_{90} is used, which is time over which we detect 90 % of all photons received from source starting at 5 % and ending at 95 %. There was also parameter T_{50} , which is defined similarly, but mostly T_{90} is used. In graphs from [27] we can notice a decrease for T_{90} around 2 s (figure 1.3). This gave idea of splitting GRBs into two groups, short GRBs (SGRB) with $T_{90} < 2$ s and long GRBs (LGRB) with $T_{90} > 2$ s [27]. Later there was a proposition for a third group of intermediate bursts with $T_{90} \sim 2$ s although any other groups of GRBs apart from long and short were not broadly accepted by the community [22, 23].

Afterglows

From the isotropic distribution a question of origin of GRBs emerged. The distribution permitted only a limited range of possible locations of GRB origins. To confirm an extragalactical nature an observation of counterpart in spectral bands such as X-rays, optical or radio was hoped for. First such counterpart in X-rays was detected by BeppoSAX in February 28, 1997 [10]. By precise localization of the prompt emission it allowed to detect

Figure 1.3: Bimodal distribution of GRB durations of prompt emission. Notice the decrease around $T_{90} \sim 2$ s

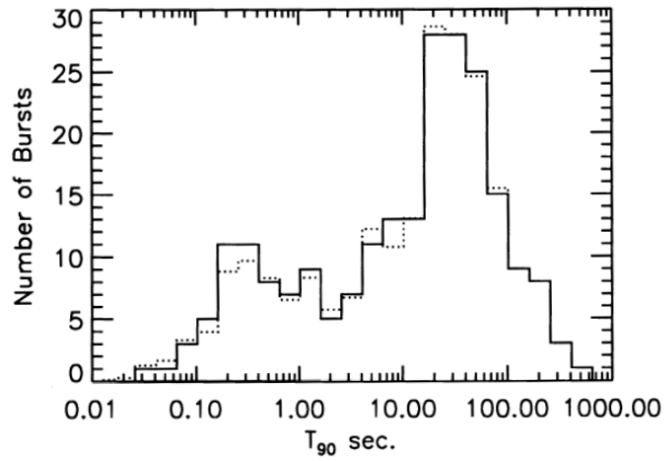
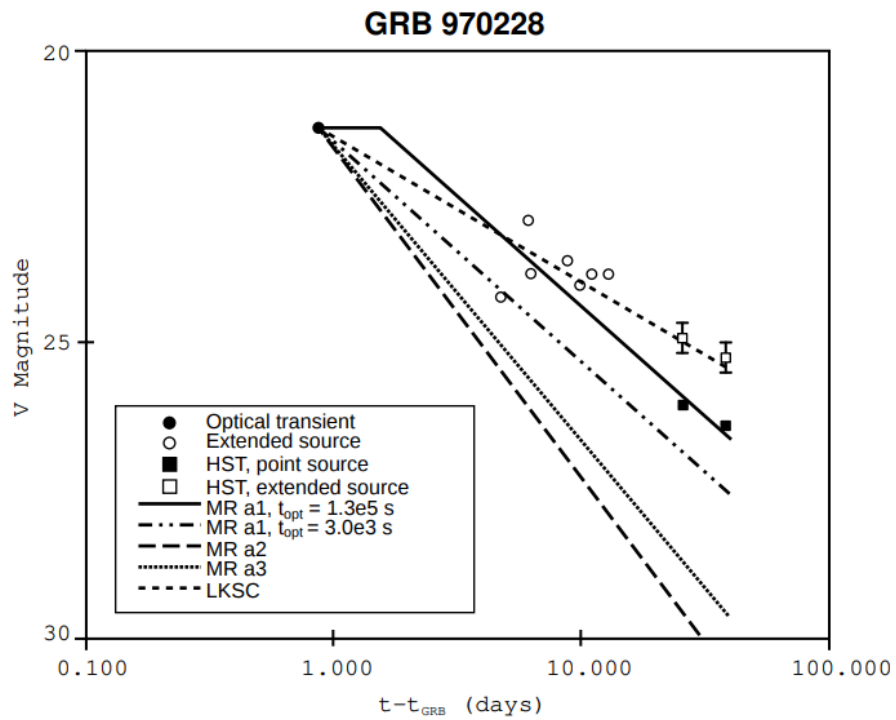
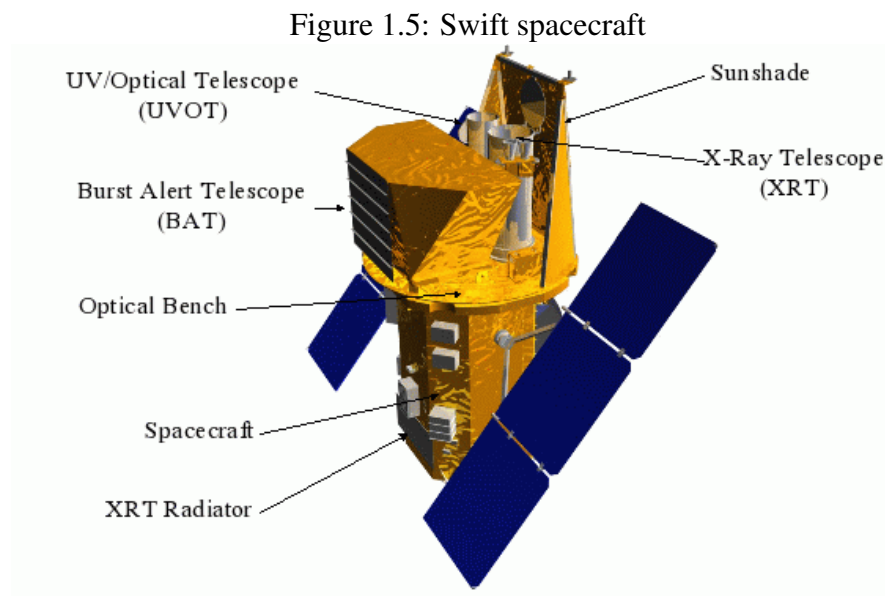


Figure 1.4: Light curve of the first ever detected optical afterglow of GRB 970228. From [38]





first optical afterglow by Hubble Space Telescope [38] – light curve is shown in figure 1.4. Soon after this breakthrough there came also a radio afterglow detection of GRB 970508 [11].

1.1.3 Swift

A breakthrough in GRB observations was a Swift mission. It was launched on November 20th 2004 on board of Delta 7320 rocket to a low-earth orbit. Its prime mission time was planned to last 2 years and to observe over 200 GRBs during that time with 7 year orbital lifetime [15], but the spacecraft is still working and operational in 2019. Main goals of this mission are [43]:

- Determine origin of GRBs
- Classify GRBs and search for new types
- Determine how the GRB evolves and interacts with surroundings
- Use GRBs to study the early universe
- Perform first sensitive hard X-ray survey of the sky

Swift helped greatly in answering many questions about Gamma-ray bursts and early universe at high redshifts. The GRBs proved to be great probes into very early universe. As an example we name a few of interesting key discoveries [42] of the Swift mission:

- Detection of GRB 090423, the most distant source spectroscopically confirmed object in the Universe at $z = 8.3$
- Measuring metallicity of star-forming regions at high redshift ($z > 5$) using GRBs

- Discovery of long-soft GRBs without associated SN
- Discovery of X-ray flares in GRB Afterglows
- Along with Fermi satellite, discovery of soft-gamma repeaters

Since we use data observed by XRT in analysis of a specific burst further in this thesis, we describe this instrument in a bit more detail. The satellite has three instruments on board

- Burst Alert Telescope(BAT)
- X-ray Telescope (XRT)
- Ultraviolet/Optical Telescope (UVOT)

which work together on detecting the source, precisely finding its position, distributing the position via GCN and measuring spectra and light curve. Some of basic parameters of these three instruments can be seen in table 1.1. Time line of events is following: 20 seconds after GRB detection, first BAT approximate position of source (1 – 4 arcminutes) is distributed and telescope starts to slew onto position. At approximately 50 seconds after detection, the GRB is acquired and observations with other instruments begin. At about 70 seconds the more precise XRT position is distributed (3 – 5 arcseconds). At 240 seconds UVOT finding chart is distributed giving the most precise position (0.3 arcseconds). At 300 seconds XRT light curve is distributed and at 1200 seconds XRT spectra is distributed. All automatic observations end at about 60 000 seconds after GRB detection.

Swift has been officialy renamed by NASA on 10th January of 2018 to Neil Gehrels Swift Observatory in honor of Neil Gehrels who died on 6th of February 2017 and had an important role in Gamma-ray Burst astronomy.

Table 1.1: Swift instruments parameters [15]
Burst Alert Telescope

Aperture	Coded Mask
Field of View	2 sr
Location Accuracy	1 - 4 arcminutes
Energy Range	15 - 150 keV
Burst Detection Rate	>100 bursts/year

X-Ray Telescope

Telescope	Wolter I
Field of View	23.6 x 23.6 arcminutes
Location Accuracy	3 - 5 arcseconds
Energy Range	0.2 - 10 keV

UltraViolet/Optical Telescope

Telescope	Modified Ritchey-Chrétien
Aperture	30 cm
Field of View	17 x 17 arcminutes
Location Accuracy	0.3 arcseconds
Wavelength range	170 nm - 650 nm

Chapter 2

A little bit of theory behind GRBs

From observational point of view, GRBs consist of a few parts: the prompt emission in gamma-rays and an afterglow which we can observe in other EM spectrum bands. Prompt emission usually lasts significantly shorter and is much “brighter” than the following afterglow which can last for days after detection. Time scale is also dependent on the type of a GRB (SGRB, LGRB). In the following model we try to outline places where these emissions could originate and what causes them to be radiated by the source.

2.1 Fireball model

Probably the most successful GRB model to describe the mechanisms behind what we observe without dependency on a progenitor and/or energy source. It is a relativistic fireball shock model that can produce a strongly beamed jet and can explain a lot of features of GRBs, it was first proposed in [35, 36]. Even though the model is independent of the details of energy source there are differences in the resulting behaviour depending on progenitors: for long bursts progenitors see section 2.3.1, for short burst see section 2.3.2. Description given here is very brief since modeling is not aim of this thesis, however, much more detailed description of the fireball model can be found in [33] and deficiencies of the model are pointed out in [19].

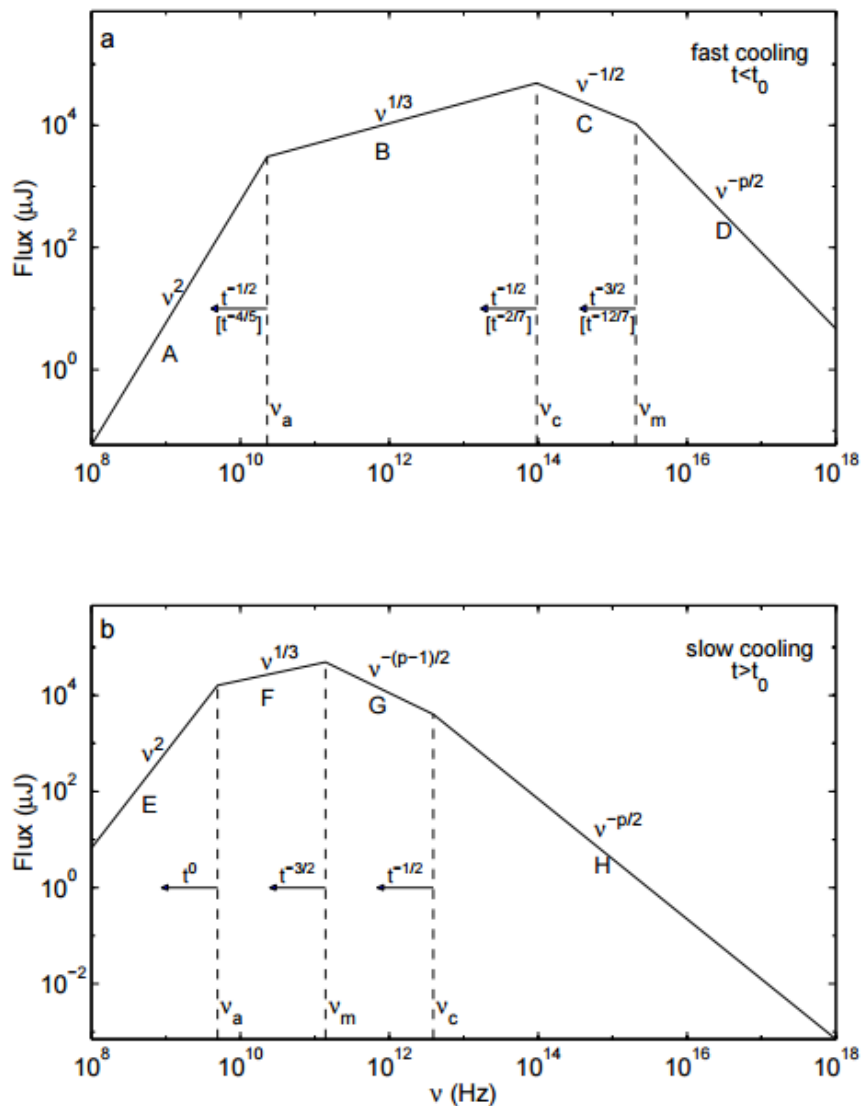
To match the observed intensities (assuming some distance corresponding to measured redshifts) a release of energy $\sim 10^{53}$ erg is required if the energy emission were isotropic, in a region which is comparable to a size of a solar mass black hole on a time scale of seconds. This suggests a relativistic release of matter with Lorentz factors of values $\Gamma \sim 10^2 - 10^3$. This condition would put an immense energy requirement which could be much easier to satisfy if the energy was beamed in a jet. The relativistic matter is converting some of its kinetic energy into electromagnetic radiation. The observed spectra are non-thermal supposed to origin in a synchrotron radiation of electrons accelerated in a strengthened magnetic field in relativistic shocks inside the jet. The spectra take form of a power-law

$$N(\varepsilon) \propto \varepsilon^{-\alpha}, \quad (2.1)$$

where $\alpha \sim 2 - 3$ at energies about 0.1 – 1 MeV. Spectrum can be seen in figure 2.1.

The central engine is supposed to be able to eject matter with different bulk initial Lorentz factors Γ which makes the shells interact with each other. This interaction which

Figure 2.1: A synchrotron spectrum created by accelerated electrons in a relativistic shock with a power-law distributon. The top image shows a Fast cooling scenarion which is expected at early times in an afterglow. It consists of four segments identified as A, B, C and D. The frequencies of breaks decrease with time as indicated, notation above arrows corresponds to adiabatic evolution, notation below arrows, in square brackets, to a fully radiative evolution. Botom image is the case of Slow cooling which is expected to happen at later times: it is always adiabatic and the corresponding four segments are identified as E, F, G and H. From [40].



is called internal shock is thought to create the prompt gamma emission. As the ejecta propagate toward the interstellar medium and interact with it, that is where so called external shock appears and most of the electromagnetic radiation of lower energies – namely X-ray, optical, radio – originates. This is called an *afterglow*.

When external shocks interact with the circumstellar medium they create back-propagating shocks that can move with a relativistic speed. Reverse shock can be a source of bright optical/UV flash [2]. Schematic overview of fireball model can be seen in figure 2.2.

As mentioned before the energy requirement is greatly reduced by beaming in a jet with an opening angle θ . If the observer is located within opening angle of the jet he can see only part of the jet which is only fraction of the opening angle, due to light aberration, which is $\sim 1/\Gamma$. In this case part of the decrease of luminosity with decreasing Lorentz factor is compensated by increased angle the observer is able to see. This stops when the Lorentz factor decreases to value such that $1/\Gamma \simeq \theta$ (see fig. 2.3) and we should observe a more rapid decrease in luminosity there on. This can explain a break in the light curve observed after about 10^5 s [30]. See figure 2.4.

The jet model reduces the energy requirement to be about an order of magnitude lower than a typical energy released in a core collapse of supernova explosion [30].

2.2 Amati and Ghirlanda relation

It is quite usual to search for correlations in new phenomena since experience proved it to be a good approach to unveil the principles behind them. In case of GRBs it was no different. There were several people trying to find such correlations and from those many relations emerged. We will focus on following two: Amati relation [4, 3] and Ghirlanda relation [17] which we will explain and discuss further.

2.2.1 Amati relation

First studies by Amati et al. were made at the moment 12 GRBs detected by BeppoSAX and GRBM had their reliable redshift estimate. It made possible to investigate trends between spectral parameters and either redshift or total radiated energy. The authors proceeded by taking time integrated spectra of all 12 sources, blue-shifted them to their source rest-frame and then fitted these spectra with a smooth broken power-law, also known as Band function [5] in the following form:

$$N(E) = A \cdot \left(\frac{E}{100\text{keV}} \right)^\alpha \cdot \exp(-E/E_0), \quad (2.2)$$

$$N(E) = A \cdot \left[\frac{(\alpha - \beta)E_0}{100\text{keV}} \right]^{\alpha - \beta} \cdot \exp(\beta - \alpha) \cdot \left(\frac{E}{100\text{keV}} \right)^\beta, \quad (2.3)$$

for $E \leq (\alpha - \beta) \cdot E_0$ and $E \geq (\alpha - \beta) \cdot E_0$ respectively. There were two relationships found: one between the α and redshift and second one which became known as Amati relation

$$E_{peak} \propto E_{iso}^{\frac{1}{2}}, \quad (2.4)$$

Figure 2.2: Scheme of a fireball model. On the left “axis” is logarithmic distance in meters. On the right, number of a phase. (1) Acceleration phase - thermal and magnetic energy is converted to baryon kinetic energy in ejecta, creating an ultrarelativistic jet beaming in a specific angle. (2) End of acceleration phase, Lorentz factor reaches maximum values, typically hundreds. (3) Ejecta starts to be optically thin. Internal energy can be radiated via quasi-thermal emission. (4) Internal shocks (CI) appear and move within the ejecta. Mass interacting with these shocks is source of prompt gamma-ray emission. (5) (6) (7) are different parts of external shock that is created from interaction of ejecta with the surroundings. (5) reverse shock (CR), that is back-propagating throughout the jet. (6) place of discontinuity, (7) forward shock (CA) which is source of afterglow emission. (8) Place where Lorentz factor decreases to a value where beaming stops being relativistic. (Atteia, Mochkovitch 2004)

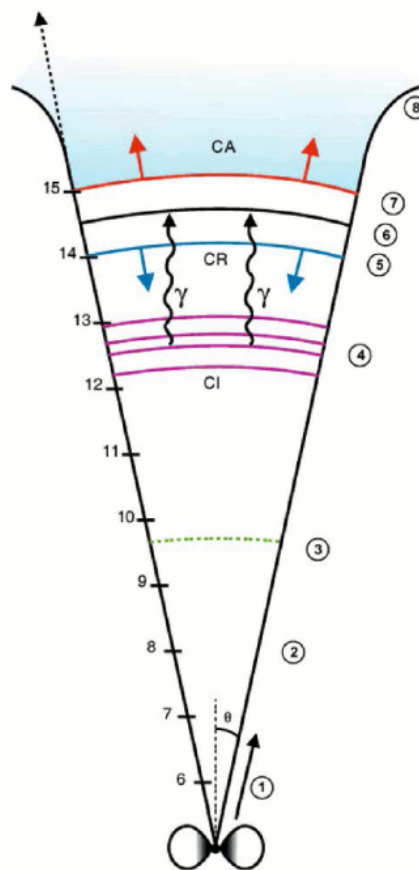


Figure 2.3: A schematic illustration showing the situation with changing visible angle depending on Γ factor. (Redrawn according to Daigne 2004).

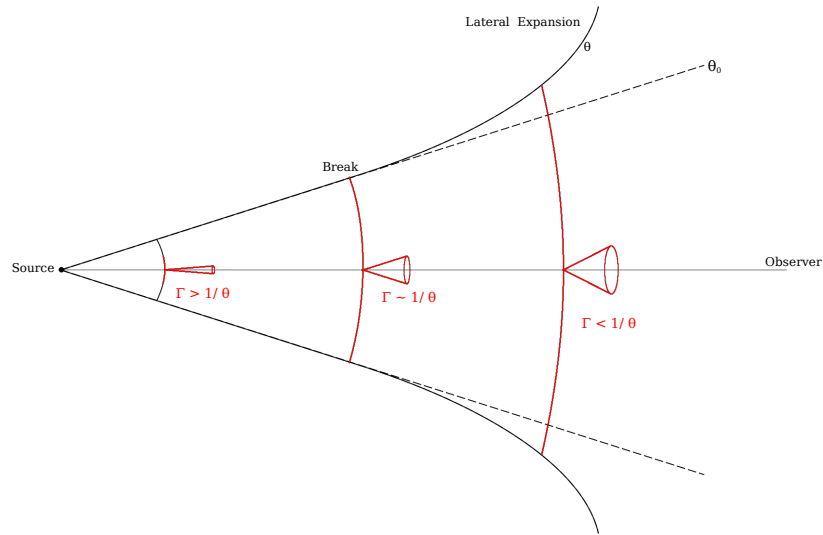


Figure 2.4: An example of a detected achromatic break in three bands of optical light curve. From [20].

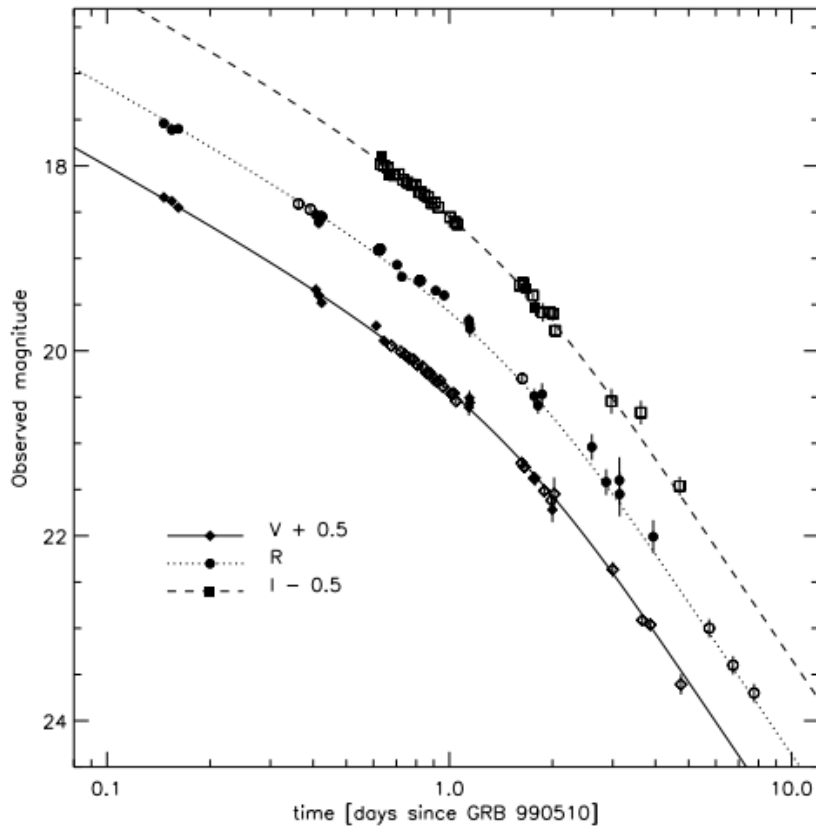
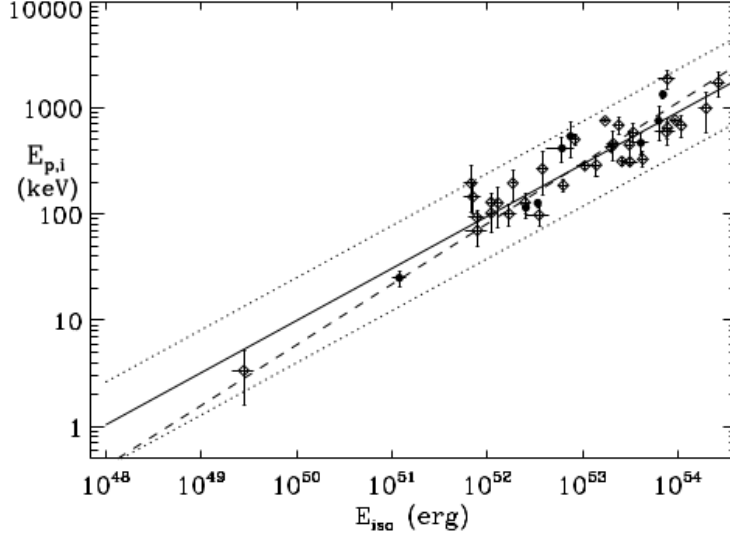


Figure 2.5: Values for E_{peak} and E_{iso} for 41 GRBs with redshift and estimates of observed peak energy. Full circles are Swift GRBs. The continuous line is fit with result of $E_{peak} = 95 \times E_{iso}^{0.49}$ taking into account source variance.



where E_{iso} is calculated as:

$$E_{iso} = 4\pi D_L^2 \int_1^{10^4} \frac{EN(E, \alpha, E_0, \beta, A)dE}{(1+z)^2}, \quad (2.5)$$

where D_L is luminosity distance calculated from Friedman-Robertson-Walker cosmological model with $H_0=65 \text{ km s}^{-1} \text{ Mpc}^{-1}$, $\Omega_M=0.3$ and $\Omega_\Lambda=0.7$. Equation 2.4 for Optically Thin Synchrotron Shock Model for a power-law distribution of electron energies as discussed in [29]. HETE-2 experiment confirmed Amati relation [4] and Swift data fit as well as can be seen in picture 2.5 [3].

2.2.2 Ghirlanda relation

Sample for analysis study done by Ghirlanda et al. 2004 [17] consists exclusively of bursts with known redshift and observed peak energy, for big part of them an estimate of jet opening angle was known from an achromatic break in afterglow light curve. It allowed them to calculate $E_{\gamma,iso}$. Relation between θ , $E_{\gamma,iso}$ and time of the jet break was given by [39] for when Lorentz factor Γ in time of break becomes $\Gamma \simeq 1/\theta$:

$$\theta = 0.161 \left(\frac{t_{jet,d}}{1+z} \right)^{3/8} \left(\frac{n\eta_\gamma}{E_{\gamma,iso,52}} \right)^{1/8} \quad (2.6)$$

where z is redshift, $t_{jet,d}$ is break time in days and $E_{\gamma,iso}$ is energy in gamma rays assuming isotropic emission. This formula only works under simplifying assumption of constant density of circum-burst medium (of number density n) and a fireball emitting fraction of

its energy in the prompt phase – η_γ . The collimation-corrected energy is calculated as:

$$E_\gamma = (1 - \cos \theta) E_{\gamma, iso}. \quad (2.7)$$

They found a tight correlation between peak energy E_{peak} and collimation-corrected energy E_γ :

$$E_{peak} \simeq 480 \left(\frac{E_\gamma}{10^{51} \text{erg}} \right)^{0.7} \text{keV}, \quad (2.8)$$

the so-called Ghirlanda relation.

They also used data from [4] and corrected the integration for redshift so the final form was:

$$E_{iso} = 4\pi D_L^2 \int_{1/(1+z)}^{10^4/(1+z)} \frac{EN(E)dE}{(1+z)^2}, \quad (2.9)$$

where for D_L calculation different values for cosmological model were used – $H_0=70 \text{ km s}^{-1} \text{ Mpc}^{-1}$, $\Omega_M=0.3$ and $\Omega_\Lambda=0.7$. The result can be seen in figure 2.6.

After Swift mission observed for about three years, there were studies finding outliers from Ghirlanda relation by Campana et. al in [7], and response with an attempt to defend the relation by Ghirlanda et. al in [18]. Nowadays it is disfavored as the necessary achromatic break in light curve is a rare sight.

2.3 Long and Short Gamma-ray Bursts origins

2.3.1 Long GRBs and SN connection

Origin of long gamma-ray bursts has been associated with end stages of a massive star, specifically collapse of its core that has been associated with supernova at least in several cases. In leading theories the remains of progenitor star after the core collapse is either BH or NS, which both can work as a central engine to create a LGRB. One of the most successful models of central engines is said to be collapsar [31, 46], where an accretion of matter onto a BH creates a bipolar relativistic jet and the gamma-ray emission originates within the jet. It also suggests sufficient kinetic energy to explosively disrupt the star. The prompt emission duration is related to the infall time of the stellar envelope [8].

The second successful mechanism is a millisecond magnetar model [44, 6]. These progenitors are extremely fast rotating and highly magnetized NS where the relativistic jets are supported by stellar confinement [6]. Periods are roughly of the order of milliseconds and B is about 10^{14-15} G . [8]

Both these models support connection of supernova and in some cases hypernova to GRBs. Illustration of a GRB-SN origin is given in figure 2.7.

GRB-SN

To get an idea about a typical character of a GRB-SN event we can specify observation conclusions from [8]. As this thesis is mostly dealing with optical observations, we focus on those. Firstly we would like to mention some of the first events that gave the direction

Figure 2.6: Solid line represents Ghirlanda relation. Full circles are collimation-corrected energies by the factor $(1 - \cos \theta)$. Empty circles are isotropic equivalents of the same sample as full circles. Dashed line is best fit to those points and dash dotted line is Amati relation from [4].

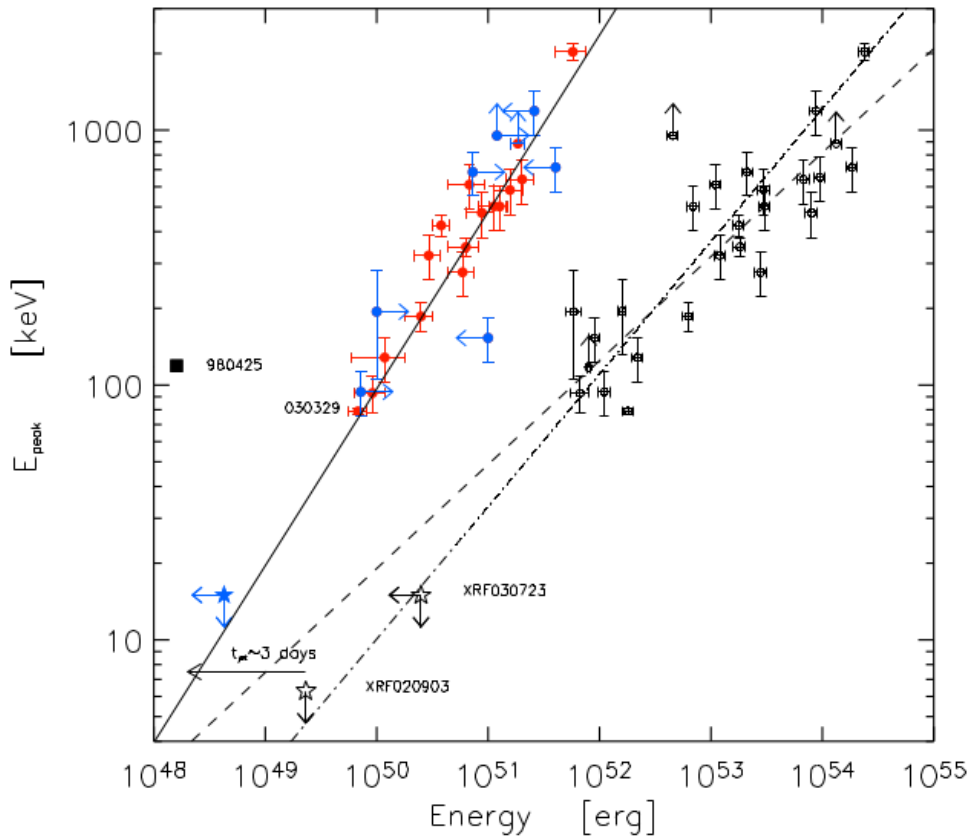


Figure 2.7: Collapsar and creation of GRB and a SN. From [32]

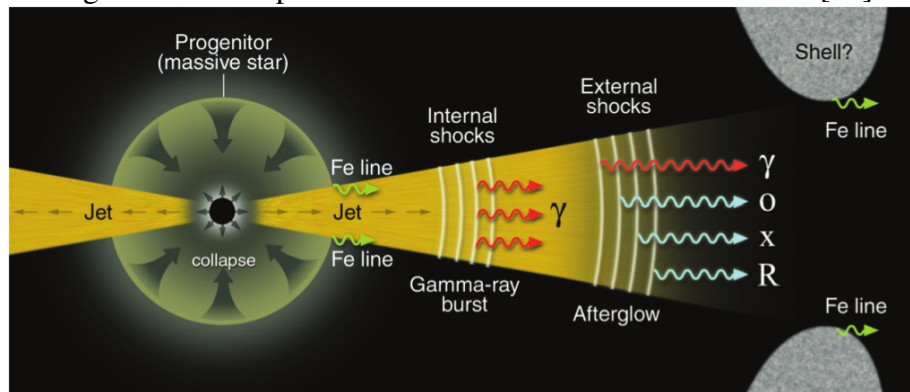
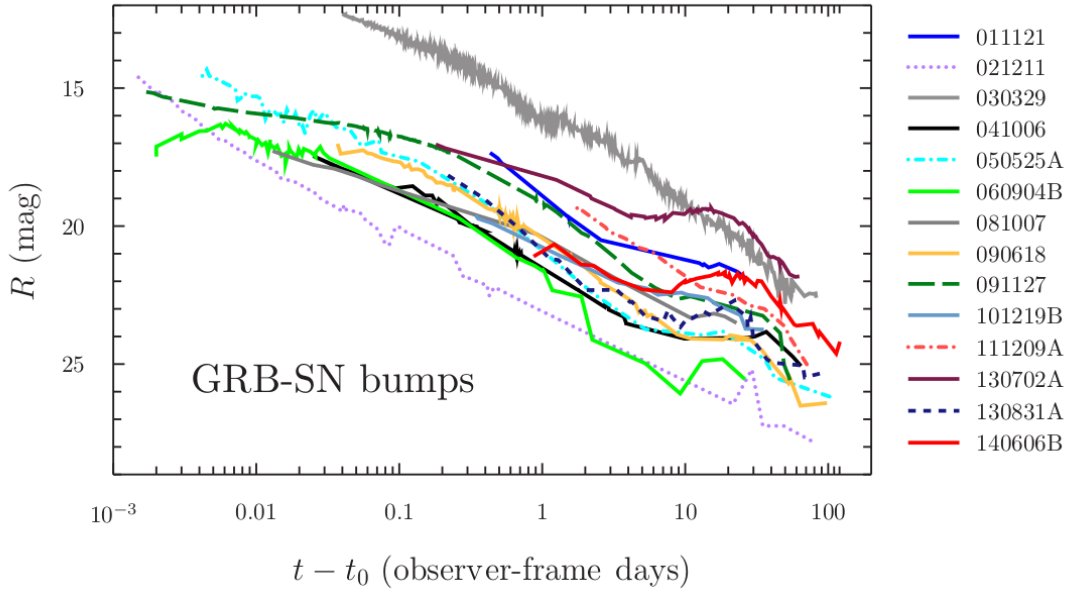


Figure 2.8: Example of light curves of GRBs associated with supernova showing the GRB-SN bumps. From [8]



to search of GRB-SN connection – the first and for a long time the only detected GRB-SN event was GRB 980425 and type Ic SN1998bw, which was also the closest GRB. The doubt it created in the question whether it is a representative of general LGRB was partially removed by a GRB 030329 and SN2003dh and after Swift was launched the number of GRB-SN associations grew bigger: GRB 060218/SN2006aj, GRB 100316D/SN2010bh and GRB 130702A/SN2013dx to name a few examples.

Typical optical light curves of GRB-SN span over more than 8 – 10 magnitudes in observer frame. Redshifts range between 0.145 and 1.006. From observed sample typical brightness is between 19.5 (GRB 130702A) and 25 (GRB 0212211) magnitudes in R band [8]. Examples of lightcurves that these data were collected from are in figure 2.8.

2.3.2 Short GRBs

For a long time it was hard to confirm the origin of short gamma-ray bursts, since before Swift there were barely any observation with a follow-up observation of an afterglow. In Swift era it became a bit clearer since many more observations of SGRBs emerged (still way less than LGRBs) so it stood for a long time on implication of studies of GRB environment. Origin of short gamma-ray burst has been thought to be mergers, namely combination of two merging black holes (BH – BH), neutron stars (NS – NS), combination of neutron star and a black hole (NS – BH), white dwarf and a black hole (WD – BH) or coalescence of binary white dwarfs (WD – WD) [28].

Detection of Gravitational-wave signal in GRBs

A very recent event, which has been an important milestone in astrophysics as well as theoretical physics, happened on October 17, 2017. A merger event, that was observed by advanced LIGO and Virgo detectors and Gamma-ray Burst Monitor of Fermi satellite, became known as first confirmed detection of gravitational waves and a complementary GRB (GW170817 and GRB170817A). The probability of these two events occurring accidentally at the same position and almost the same time is 5×8^{-50} , which confirms neutron star mergers as at least one of the origins for short GRBs [1]. Another important result was that this short GRBs was closest SGRB detected (some 2 – 6 magnitudes less energetic) which can place a new demand on detection limits for GRB missions to expand the amount of detected SGRBs in the future.

Chapter 3

Optical observations

In this thesis we mainly focus on observing optical counterparts of GRB afterglows. For acquiring observations of these afterglows mainly ground based observations are done. We describe a related system that is tightly connected to GRB follow up observations, the telescope that was used to acquire our optical data – D50 – and a few other topics related to optical observations of GRBs and CCD astronomy.

3.1 GCN/TAN

It might be a bit unusual to put GCN network into an optical observations chapter, but as most follow-up observations are done by ground optical telescopes we find it fitting as the main instrument used in this work to get data was D50 in Ondřejov, which uses the GCN Notice system for GRB alerts. It started as BACODINE, a real-time transmission of data from CGRO–BATSE to observatories and any other interested part for follow-up observations although the uncertainty with which BATSE could determine position of source could be up to 10° , however it would still increase chance of detecting GRB in other bands and helping to solve the mystery of GRBs. Later when more instruments and missions were added the name was changed to more general GCN and later even further to GCN/TAN [14]. GRB Coordinates Network (GCN) or Transient Astronomy Network (TAN) consists of two parts:

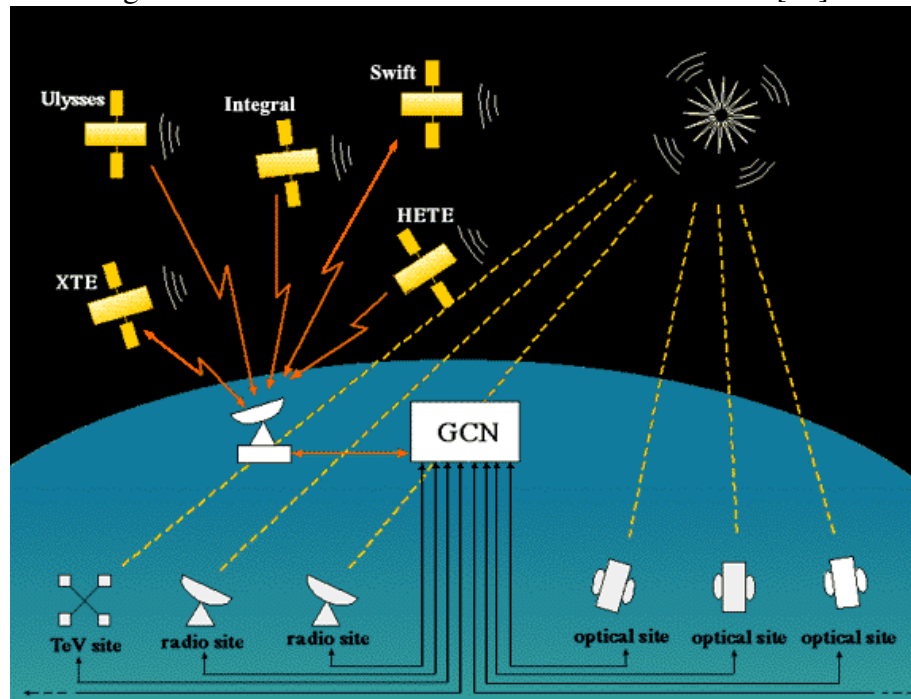
- GCN Notices
- GCN Circulars

3.1.1 GCN Notices

This part of GCN/TAN distributes the location of GRB/transients detected by various spacecraft to enable follow-up observations. At this time some of the spacecrafts/missions/instruments that detect sources are:

- Swift
- INTEGRAL

Figure 3.1: Illustration of GRB Coordinates Network[13]



- IPN
- KONUS
- AGILE
- Fermi

and some others. It is worth mentioning some of the previous missions that used to be part of the GCN Notice network, as they had significant impact on GRB research, but ended their mission: CGRO, BeppoSAX, HETE, Suzaku. The most significant feature of this network is that there is no human interaction necessary for these notices to distribute so the delay between detection and information being sent ranges between 2 – 10 s. The distribution is possible using varying protocols one of which may be a simple email message or TCP/IP socket distribution. This usually allows to find the transient soon after it was discovered and located for early follow-up observations [14]. An illustration of GCN can be seen in figure 3.1.

3.1.2 GCN Circulars

A second part of the GCN/TAN has its purpose in sharing information via email/message style notifications from GRB community which can contain information confirming detection of the specified GRB with their instrument, more precise localization, some early analysis of GRB properties, spectroscopy and redshift measurement and other GRB related

Figure 3.2: D50 Telescope. Credit: Martin Jelínek



information. It is possible to access GCN Circulars archive and look for information related to specific GRBs that was shared using GCN Circulars. An example of information sent via circulars can be seen for GRB 131030A in section 5.1.

3.2 D50

D50 is a robotic telescope built by HEA (High-Energy Astrophysics) group of Astronomical Institute CAS at Ondrejov with a goal to refurbish an old telescope at low-cost for follow up observations of GRBs and other objects of high-energy astrophysics. Main parameters of this telescope can be found in table 3.1 and optical arrangement is shown in figure 3.3. [34]

It began its new journey in the beginning of year 2008 and had its first successful detection of an optical afterglow of GRB on 30th of April 2008. GRB080430 was detected one hour after the satellite trigger with magnitude of 18.9 mag in R filter. Image of the detected source can be seen in 3.4. [34]

Table 3.1: D50 telescope parameters [34]
D50

Optical setup	Newtonian system
Primary mirror diameter	500 mm
Secondary mirror	100 mm
Field of view	20×20 arc minutes
Focal length	1975 mm (effectively 2277 mm using ParaCor optics)
CDD resolution	1024×1024 pixels
Available photometric filters	B,V,R,I
Limiting magnitude	18.9 mag at 3σ for 60 s in V band
Slew speed	0.6 degrees/sec
Attached wide field camera	
Field of view	1.58×1.05 deg
CCD resolution	1536×1024
Limiting magnitude	16.2 mag at 3σ for 60 s

Figure 3.3: Optical arrangement schema of D50 telescope [34]

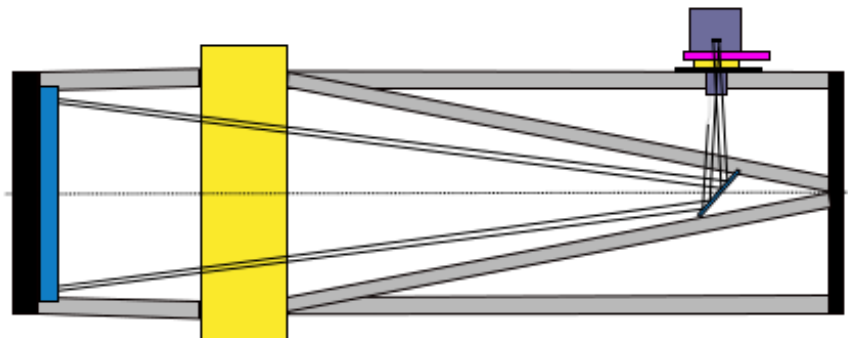
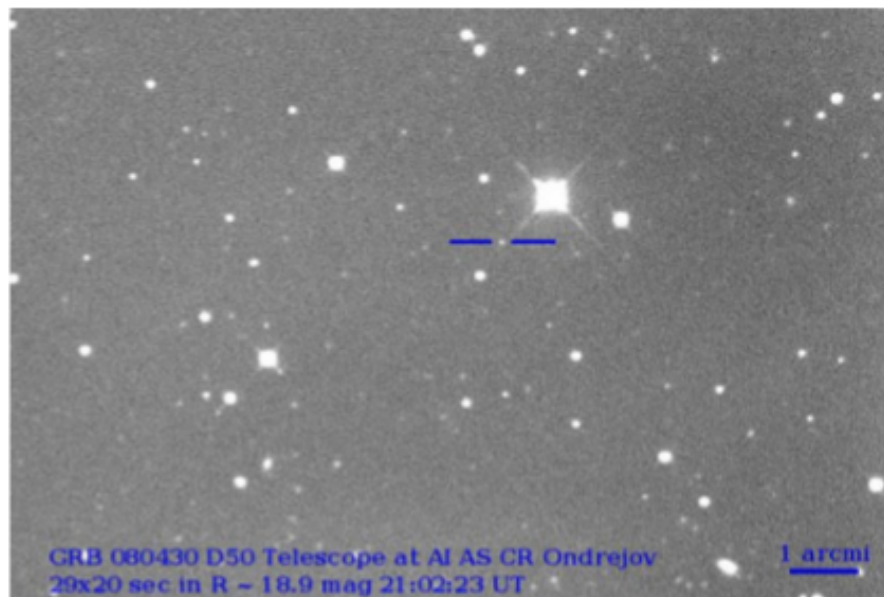


Figure 3.4: First detection of D50. GRB080430 [34]



Optical data we use in this thesis are acquired using this telescope as a follow up of Swift BAT trigger distributed via GCN. It is important to mention that observations with this telescope are automated and the telescope control is done via RTS2 Software [37]. The operation mode is usually based on a list of scheduled observations of targets which it goes through during observing nights. If a trigger appears it terminates ongoing observation and proceeds to observe the trigger target.

D50 is a part of a network of robotic telescopes called GLORIA (GLOBal Robotic-telescopes Intelligent Array) which aims to bring possibility to observe or access data to anyone interested in astronomy with a web browser, not just professional astronomers. It is worth mentioning other robotic telescopes that are part of the project: BOOTES1/2 in Spain, BOOTES3 in New Zealand, FRAM in Argentina, Pi of the Sky 1 in Chile, Watcher in South Africa, REM in Chile just to name a few, in total there are 18 telescopes (as of 2014). On an obvious purpose the telescopes are located in many different parts of the globe. [9]

3.3 Ground based optical observations

3.3.1 CCD Image reduction

A CCD image is a matrix of numbers where X, Y are positions of pixels and each pixel has its value of intensity or brightness. After the exposure of CCD chip photons are converted to electrons – this signal follows Poisson statistics, however there are other sources of signal that do not represent observation data and need to be corrected for. The goal is to process the image in a way that we reconstruct the original signal.

This is done by some arithmetics using calibration images:

- **Bias** – electrical offset added to ccd, in some cases the offset is constant and in others not in which case it has to be subtracted. Correction frame is done by exposure of zero seconds with shutter closed.
- **Dark current** – CCD thermal signal. Has to be scaled to time of exposure to be subtracted, it scales with exposure. Correction frame is done by exposure of given time and closed shutter.
- **Flat field** – pixels on the CCD can have different responses, that can depend on spectral band used and position of the source photons are coming from. Correction frames are created with exposures of evenly illuminated surface or a twilight sky. Correction is applied by a division while flat is normalized by its mean value to preserve original signal intensities.

The way correction images are applied to a data image is following:

$$\text{corrected image} = \frac{\text{raw image} - \text{bias} - \text{dark}}{\text{normalized}(\text{flat} - \text{bias} - \text{dark})}, \quad (3.1)$$

flat also has to be corrected for dark current and bias. However in optical observations used in this thesis the correction for bias is not necessary. So the formula we use is simplified by leaving out the bias images.

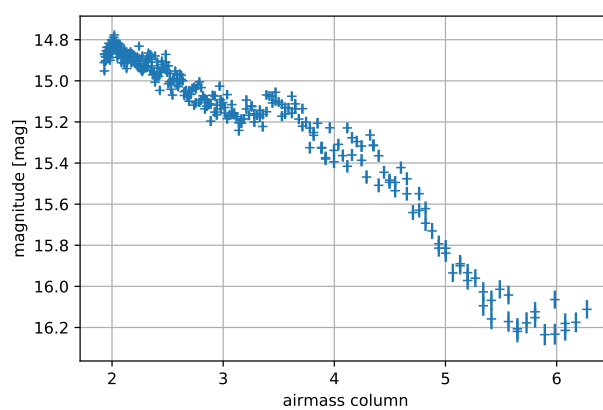
$$\text{corrected image} = \frac{\text{raw image} - \text{dark}}{\text{normalized}(\text{flat} - \text{dark})}. \quad (3.2)$$

Both dark and flat correction images are created by combining several exposures of images described above. The method we use to combine dark image is to calculate median values for each pixel from all input dark exposures. The combining method for flat and normalization is done by first subtracting resulting combined dark image from each of the input exposures and then median combining the images in the same way as for dark images; finally we divide each value by the mean value of the whole image.

3.3.2 Airmass

One of the other caveats of ground based optical observations is the effect of air mass on reducing the magnitude, it can clearly be seen in light curves of calibration stars (see figure 3.5) we use for calibrating observations in Chapter 5. To account for this shifting zero magnitude of images when is done when performing photometric calibration which removes the effect of changing airmass column to the source (more information in section 4.3.2). The effect is more delicate for afterglow observations used in chapter 5 which were performed without any optical filter (the atmospheric absorption effect affects different wavelengths differently).

Figure 3.5: Effect of increasing airmass on a light curve. Plotted light curve is of a star with constant brightness.



Chapter 4

GRBLC

GRBLC is a python package made with intention of reducing the amount of time spent on data reduction and image processing of automatic gamma-ray burst observations done e.g. by robotic telescopes at Astronomical Institute CAS in Ondřejov, D50 and BART. This code was created to primarily process data from aforementioned telescopes but should be easily usable with observations from other devices. It was written with intention to eventually automate the whole process to the point where user would get the final product without having to interfere with the process at all. At this stage it's necessary to input data and do automated reduction, photometry and stacking of low signal to noise ratio frames. Also can be used e.g. in Jupyter¹ notebook to use only parts of the package to do the data reduction and photometry by hand using few easy steps.

This part focuses on how to use all features this package has to offer, rather than explaining the theory behind it, for that see [4.3](#)

4.1 Installation

To use this package go to <https://github.com/foodiq-pk/grblc> and download it. You can either install it as a python package by moving it to a directory with packages of your python distribution or simply add path with location in your import section while writing a script or using a notebook as shown in example. After that you can import as shown in examples further in this chapter.

```
import sys
sys.path.insert(0, "/path/to/grblc/folder/")
```

4.2 Structure

The GRBLC package is divided into two main parts.

- Data processing

¹The Jupyter Notebook is an open-source web application that allows you to create and share documents that contain live code, equations, visualizations and narrative text.

- Image processing

In data processing there are data structure classes representing images and objects in the sky e.g. stars and grbs. Each `SkyObject` or `Image` object has its attributes and parameters discussed further in 4.2.1. Another part of data processing are data handlers; for handling database input and file input as well as downloading information about objects from on-line catalogues – available at the moment are APASS or and more described in 4.2.2.

Image processing part consists mainly of transformers. Each transformer has different functionality but applies in a same manner to image. Examples might be dark and flat correction transform or photometry transform but all of them are more described in part 4.2.3. There is also separate part for stacking images. Each transformation of image needs a previous information contained in the `Image` object. It could be e.g. photometry requires corrected data, or zero magnitude shift transform requires photometry done beforehand.

4.2.1 Objects

In this section we describe two important classes for representing stars and GRBs – `SkyObject` and images – `Image`.

`SkyObject`

Object container for representing stars and GRBs. It offers possibility to draw light curves of an object. It is always necessary to pass right ascension, declination, catalogue magnitude, catalogue filter and id when creating star object. To create a star object see example. However most of the time the star type objects are created automatically when querying for objects around GRBs (see section 4.2.2).

```
from grblc.data_processing.datastructures import SkyObject
star = SkyObject.star( id="1",
                      ra=250.3, dec=45.1,
                      catalog_magnitude=(12.2, 0.02,
                      cat_filter = "V")
```

To draw a light curve for object you use method called `plot_light_curve(images)`. Parameters of this function allow it to produce plots with or without errorbars on both axes and plotting either raw data right after photometry or after calibration. So far y axis is magnitude and x axis is time in Julian days. It is possible to plot a light curve for each object not just GRB in the following example. Note that to draw a light curve you need to have photometry done, and for shifted light curve shift must be calculated as well.

```
skyobject.plot_light_curve(image_list,
                           type="shifted", # "raw"
                           timerr=True,
                           magerr=True)
```

It is also possible to get the data as numbers instead of a plot. To do so you can call either `get_raw_light_curve(image_list)` or `get_shifted_light_curve(image_list)`. All four parameters are assigned as in the following example.

```
raw_lc = skyobject.get_raw_light_curve(image_list)
time, time_err, mag, mag_err = raw_lc

shifted_lc = skyobject.get_shifted_light_curve(image_list)
time, time_err, mag, mag_err = shifted_lc
```

Object contains methods to get its parameters comfortably.

```
SkyObject.get_id()
SkyObject.get_type()
SkyObject.get_ra()
SkyObject.get_dec()
SkyObject.get_trigger_jd() # grb only
SkyObject.get_catalog_magnitude() # star only
SkyObject.get_catalog_filter() # star only
SkyObject.get_raw_light_curve(imgs)
SkyObject.get_shifted_light_curve(imgs)
```

GRB is stored as `SkyObject` but has slightly different attributes. As GRB doesn't have catalogue magnitudes it requires its name, right ascension, declination and time of trigger in Julian date, instead. Function used to create a GRB object is shown in the following example.

```
from grblc.data_processing.datastructures import SkyObject
grb = SkyObject.grb(name="GRB12345B",
                    ra=345.2,
                    dec=-5.42,
                    trigger_jd=214566.215689)
```

Image

Image is an object container for storing and manipulating FITS images. It always has information about FITS file, exposure length and Julian date of its beginning and type of image, be it dark, flat, raw data image or corrected. It also contains methods to easily retrieve these parameters and to get processing parameters e.g. photometry of objects in the image or its zero magnitude shift. You should use one of the available data handlers to create `Image` objects. Attributes you can get from these objects are following:

```
Image.get_id()
Image.get_type()
Image.get_path()
Image.get_time_jd()
Image.get_exposure()
Image.get_photometry() # from Phot transform
Image.get_src_flux() # from Phot transform
Image.get_sky() # from Phot transform
Image.get_shift() # from Shift transform
Image.get_shifts() # from Shift transform
Image.get_stack() # source images of stack
```

4.2.2 Data handling

This package has its own module for handling data. It is easier for user to just call a specific data manager or handler and let it do the work creating `Image` and `SkyObject` lists that

are later used for creating and calibrating light curves. It allows loading single image or multiple images from a folder, loading images and object along with additional processing information from a database of any kind if it contains required tables and structure. Saving image and object information to database and querying for object data in on-line catalogues.

Each handler contains at least method `get_list()` which will return image list or object list that loads objects or images based on parameters given when creating the handler. More on how to use handlers in specific handlers sections.

File handler

Handler for loading images from files and folders. Creates image list which is used as a container for `Image` objects that are then passed to other functions and procedures. To create a `FileHandler` you need to specify two things. First is a folder from which you want to load images and second is type of image data you are loading which can be either flat, dark, data or already corrected data. Keywords for this are: "flat", "dark", "data", "ddata" for dark corrected images or "dfdata" for dark and flat corrected images for which you can alternatively use "cdata" standing for corrected data. Optionally you can specify smaller group fitting a query to load only some of the images in given folder. After creating `FileHandler` object you can call `get_list()` method to create a list of `Image` type objects with all their relevant data loaded from FITS images in that folder. Example follows.

```
from grblc.data_processing.datahandlers import FileHandler

fh_dark = FileHandler(folder="path/to/darks",
                      query="*.fits",
                      type="dark")
darks = fh_dark.get_list()

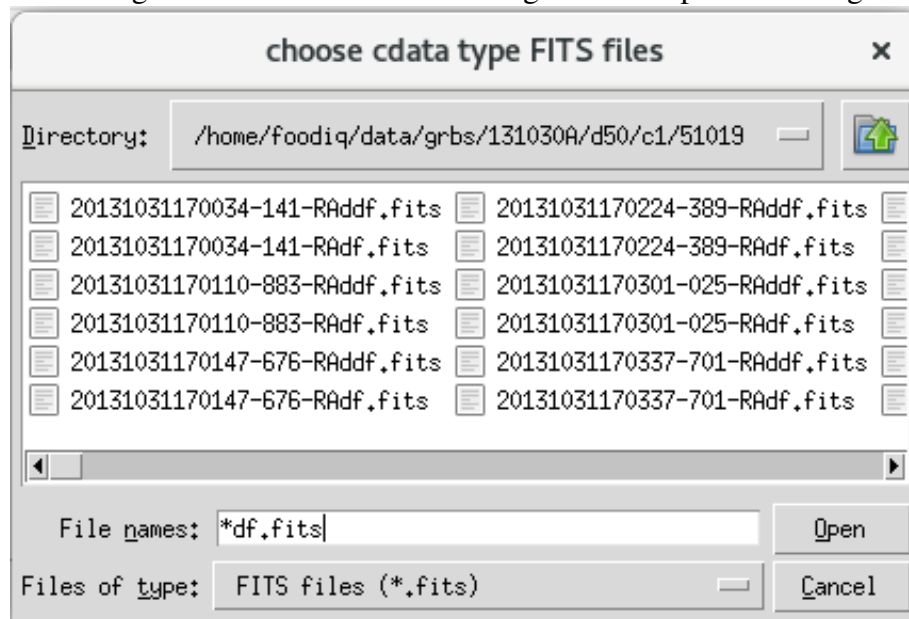
fh_flat = FileHandler(folder="path/to/flats",
                      query="*.fits"
                      type="flat")
flats = fh_flat.get_list()

fh_raw_data = FileHandler(folder="path/to/images",
                          query="*.fits",
                          type="data")
raw_data = fh_raw_data.get_list()

fh_corrected_data = FileHandler(folder="path/to/corr/images",
                                query="*.fits",
                                type="cdata")
corrected_data = fh_corrected_data.get_list()
```

For a more GUI oriented user there is option to use a handler with dialog window that will prompt user for images. Only thing you need to specify when creating `FileHandler Dialog` object is the data type you intend to load. After that by calling `get_list()` method you open dialog window and select the images.

Figure 4.1: Dialog window of FileHandlerDialog with example of filtering image input



```

from grblc.data_processing.datahandlers import FileHandlerDialog

fhd_darks = FileHandlerDialog("dark")
darks = fhd_darks.get_list()

fhd_flats = FileHandlerDialog("flat")
flats = fhd_flats.get_list()

fhd_raw_data = FileHandlerDialog("data")
raw_data = fhd_raw_data.get_list()

fhd_corrected_data = FileHandlerDialog("cdata")
corrected_data = fhd_corrected_data.get_list()

```

It is possible to use query in the dialog window to reduce amount of results show as you can see in image 4.1.

Object handler

Handler designed to return objects in a field around target GRB. At the moment it is possible to choose querying for objects in two catalogues - one being APASS[21] and the other NOMAD[47]. APASS is recommended for use because it contains more precise information about magnitudes.

When creating `ObjectHandler` you specify which target GRB you are querying objects around. It is also possible to adjust limit of objects you get which is by default set to 100. When calling `get_list()` method to get objects you can also specify radius in degrees in which to query for objects and their limiting magnitude; these parameters are set to 0.1 degrees and 16 magnitudes, respectively, as a default which is based on images from D50 in Ondrejov.

```
from grblc.data_processing.datahandlers import ObjectHandler

oh = ObjectHandler(grb)
object_list = oh.get_list(mag_limit=16.0,
                          catalog="APASS", # or "NOMAD"
                          radius=0.1)
```

Database handler

Handler for saving and loading your working progress or just saving results for later use if you want to. It is possible to save information about images, objects, magnitudes on specified images, image calibration magnitude shifts, stacked images, source flux and sky flux. There are two tables containing this information.

- images
- skyobjects

Table with images contains identifier, information about location of image file, exposure start julian date, duration of exposure, type of data, shift of zero magnitude and magnitude of grb in that image along with flux information (counts flux) and sky values. Along with additional column containing information about photometry results, specific shifts of objects in an image and any other relevant information user might input on his own. The only requirement is that is is written to the Image objects as a "processing_parameter" dictionary entry and contains only basic data structures for it to load from and save to database correctly.

Table with skyobjects contains identifier, right ascension, declination and catalogue magnitude. As images table, this can contain any additional information specified by user if he wishes so as a dictionary entry in "processing_parameters" attribute.

Saving images as database entries

One usages of `DatabaseHandler` is to save data after some analysis or image correction. To save to a specific file or database you have to create a `DatabaseHandler` with information about the target database. In example you can see how to save to a "sqlite3" database file.

```
from grblc.data_processing.datahandlers import DatabaseHandler

dh = DatabaseHandler(connector=sqlite:///relative/path/db.db)
# alternatively:
# dh = DatabaseHandler(connector=sqlite:///full/path/db.db)

dh.save_objects_and_images(image_list, object_list)
```

After saving the file is transferable between sessions. It should be possible to save to a live database containing the same structure as described in previous section. Entries in database with same ID (understand images and skyobjects) will be updated with the latest information saved to given database and old information will be lost, so be mindful to specify different target database or copy the saved data if you wish to keep them along with the new ones!

Loading

Second usage of database handler is to get image and object lists as with other handlers. For this matter create a `DatabaseHandler` with information about target database to load from. Database has to have the structure specified earlier. After calling method `get_list()` you need to specify two variables first being for image list and second for object list.

```
from grblc.data_processing.datahandlers import DatabaseHandler

dh = DatabaseHandler(connector=sqlite:///relative/path/db.db)
# alternatively:
# dh = DatabaseHandler(connector=sqlite:///full/path/db.db)

loaded_images, loaded_objects = dh.get_list()
```

4.2.3 Operating with CCD data

All image modifications, be it correcting for dark current or flat fielding and image, doing photometry or calibrating results of photometry is done using objects called transformers. This design allows for chaining transformers behind each other to get effect of all selected transformer on an image in one go, making it faster and easier to apply them to images. There are at the moment several transformers that will be discussed further.

Transformer and TransformerManager

For chaining transformers there is a class called `Transformer`. It manages transformers and applies them in succession on an image that is then returned. It creates copy so you won't lose your former image, but get new modified image afterwards. It takes in a list of transformers that you want to apply. Be mindful of their order if you apply them separately as you won't be allowed to do photometry on non-corrected images or calibrate a photometry without doing one. Each transformer has its required pre-steps which can be done using the package (dark or flat field correction) or just specified when loading images that the steps of correction were already applied. Photometry and calibration (magnitude shift) information is only provided by their specific transformers. In example you can see usage of three transformers that are doing dark correction, flat field correction and photometry of objects given.

```
from grblc.image_processing.transformators import Transformer, DarkTransform,
    FlatTransform,
from grblc.image_processing.transformators import PythonPhotPhotometryTransform
    as PhotTransform

transform_list = [DarkTransform(master_dark),
                  FlatTransform(master_flat),
                  PhotTransform(object_list)]

transformator = Transformer(transform_list)

processed_image = transformator.apply(input_image)
```


However if you are using only this package for correcting images it is advised to apply dark correction to flat images before creating master flat image. That can be done as in example.

```
from grblc.image_processing.transformators import TransformatorManager,
    DarkTransform

transform_list = [DarkTransform(master_dark)]

transformator_man = TransformatorManager(transform_list)

flats_d = transformator_man.apply_transformations(flats)
```

After that usage is similar as with `DarkTransform`, initialize it with normalized master flat image and then use it in `TransformatorManager` or with other transformators in a sequence.

```
from grblc.image_processing.transformators import TransformatorManager,
    FlatTransform

transform_list = [FlatTransform(master_flat)]

transformator = TransformatorManager(transform_list)

images_flat_corrected = transformator.apply_transformations(image_list)
```

4.2.4 Photometry

Presently there are two photometry procedures. First is an IRAF **daophot** [41] procedure run through PyRAF and needs you to have IRAF and PyRAF which if you have allows using this procedure to do photometry as if you did in IRAF, however setting it up properly can be a tedious task which is why this method is marked as deprecated and is not recommended for use. It is there however for users which would prefer doing it this way.

Second is from a python transcribed daophot from IRAF – PythonPhot.[24] The installation for this is far easier and should allow the same quality of photometry as daophot in IRAF. We recommend doing photometry this way.

Both photometry transforms require having dark and flat field correction applies beforehand. Unlike previous transforms Photometry needs an object list of stars/GRB to do photometry on. It will only do photometry on objects that are present in an image and ignore rest, if any objects out of the image are contained in given object list.

PyrafPhotometryTransform

This photometry uses PyRAF procedure DAOPHOT. [41] However as mention before we encourage usage of the other photometry procedure. It is possible to get all the output files as created by PyRAF for other information about the objects, but it requires modifications to package's code so its only recommended for advanced users. At this stage this photometry provides magnitude measurement of objects specified on input. Example of usage is as follows

```

from grblc.image_processing.transformators import PyrafPhotometryTransform as
    PhotTrans
from grblc.image_processing.transformators import TransformatorManager

phot_trans = [PhotTrans(object_list)]

phot_man = TransformatorManager(phot_trans)

phot_images = phot_man.apply_transformations(image_list)

```

PythonPhotPhotometryTransform

Photometry is done using PythonPhot package [24]. It claims to be DAOPHOT-type photometry procedure from IDL AstroLib. The module we use is aperture photometry.

This transformator requires corrected data as input, list of objects in the picture (can be also outside of the bounds of picture but photometry wont be calculated). You can specify aperture in configuration file.

It provides a photometry parameter for `Image` object, which behaves as a dictionary: if you enter id of object you will get magnitude along with its affiliated error. It also provides information about background flux and source flux, source being the GRB around which the objects were queried for². You can get those other parameters by getting Images' attribute `src_flux` and `sky`. Usage is as follows with examples of getting other information from Image later.

```

from grblc.image_processing.transformators import PythonPhotPhotometryTransform
    as PhotTrans
from grblc.image_processing.transformators import TransformatorManager

phot_trans = [PhotTrans(object_list)]

phot_man = TransformatorManager(phot_trans)

phot_images = phot_man.apply_transformations(image_list)

phot_images[0].get_src_flux()
phot_images[0].get_sky()

```

4.2.5 ShiftTransform

`ShiftTransform` is used as a means for calibrating lightcurves. Requires `Image` list objects that `PhotometryTransform` has been applied to (in this case it can be either of both mentioned above). It uses catalogue magnitude values of objects in the image field and uses them to calculate magnitude shift of the image as a whole and makes it possible to shift this curve by the specified amount. It also calculates affiliated error. Usage is as follows:

```

from grblc.image_processing.transformators import ShiftTransform
from grblc.image_processing.transformators import TransformatorManager

shift_trans = [ShiftTransform(object_list)]

```

²It is necessary for GRB to be first object in the input list to be defined as the (principal) source.

```
shift_man = TransformatorManager(shift_trans)

shifted_images = shift_man.apply_transformations(image_list)

shifted_images[0].get_shift()
shifted_images[0].get_shifts()
```

As you can see in example, there are two getters for different values, one contains calculated shift of the image magnitudes (amount by which the resulting light curve is shifted) and the second dictionary for differences between catalogue magnitude and photometry output from which the first one is calculated.

4.2.6 Image stacking

Image stacking is a separate module as it works on a slightly different basis from other transformers. It takes image list with photometry and optionally a GRB target allowing user to plot images that were selected for stacking. Algorithm calculates expected value of signal to noise and selects images based on limitation given by user in method `select_images_to_stack()` with a signal to noise limitation. After this method is run user can visualize images selected for stacking by calling `plot_stack_prediction()` and see example result in as figure 4.2. Once user has selected images it is possible to call `stack_images()` method to run the stacking procedure. There is option to run procedure on multiple cores to speed up the process on stronger computers, to do so use `stack_images_multicore()` instead where you can specify the number of cores to be used, the amount defaults to one and is then equivalent to the regular method. Once finished, to get complete list of unstacked images and stacked images user can call `get_list()` method to get time sorted image list with stacked images.

```
stack = StackingManager(image_list_with_photometry, grb)
stack.select_images_to_stack(signal_to_noise_limit)
stack.plot_stack_prediction() # optional
stack.stack_images()

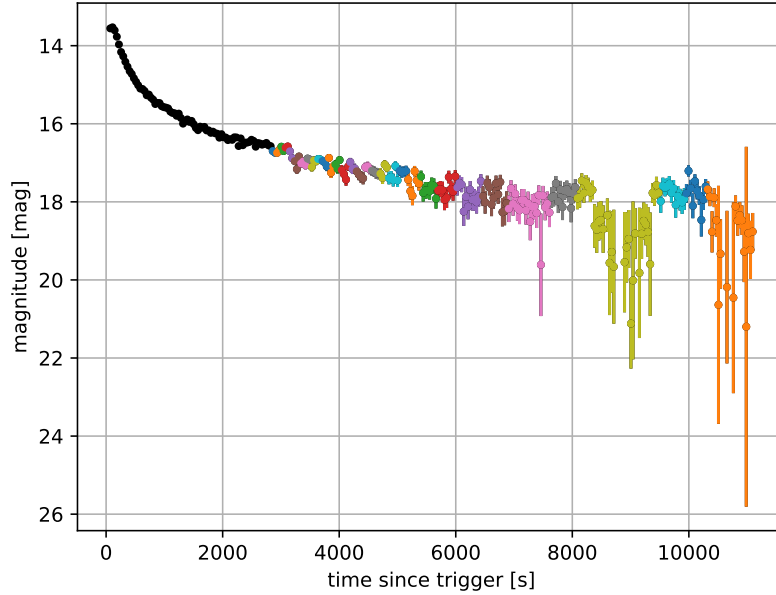
stacked_list = stack.get_list()
```

Images that were stacked will have a new attribute called `stack` returned by `get_stack()` which contains paths to stacked images along with their filenames. Stacked images are also by default created in a temporary folder, to move them/save them you can use method `save_stacks()` and specify folder to which to move these images. The stacked list then has new path info in it. This method has to be run before getting the final image list if you want it to change the path of the files to the new location.

The stacking procedure also allows accessing the pre-stacking data, which is list of image lists to be stacked into single image in attribute `to_stack` which corresponds with the predicted signal to noise ratios in attribute `sn_prediction` or `get_sn_prediction()` and other listed in following example.

```
stack.grb
stack.single_images
stack.to_stack
stack.get_sn_prediction()
```

Figure 4.2: Example of selected images for stacking



4.3 Procedure descriptions and algorithms

In this part we describe procedures or algorithms used to create methods in previous part. It is described to a degree which we believe can bring a bit of light to how it was done, in simpler tasks we settle for a brief explanation since there are ways of doing it already and are broadly know however for some custom methods we go into a bit more detail. For some of the externally used packages we confirm that they behave in a way we would expect.

4.3.1 DarkTransform and FlatTransform

As was briefly described in theoretical part of this thesis, the DarkTransform and FlatTransform creates master images for correction by median combining input images. For master dark image, only images of corresponding exposure are selected. When applying dark correction to a data or flat frame it is scaled to exposure of corrected frame. For DarkTransform the procedure does:

$$dark\ corrected = raw\ image - \frac{exp_{raw}}{exp_{dark}} master\ dark, \quad (4.1)$$

where exp_{raw} and exp_{dark} are exposures of raw image and master dark, respectively. FlatTransform normalized master flat is created as:

$$master\ flat = med(flat),^3 \quad (4.2)$$

³median value for each pixel in all images

$$normalized\ maste\ flat = \frac{master\ flat}{mean(master\ flat)}^4. \quad (4.3)$$

4.3.2 Shift Transform

Our way of calibrating photometry, for which we decided based on our observations being unfiltered, is shifting the magnitude of a whole image by value calculated from calibration stars.

Firstly we get values calculated by photometry in given image and subtract them from catalogue magnitude to get differences for all the stars and compute their combined errors:

$$shift_{star} = m_{star,catalog} - m_{star,photometry}, \quad (4.4)$$

$$\sigma_{shift,star} = \sqrt{\sigma_{star,catalog}^2 + \sigma_{star,photometry}^2}. \quad (4.5)$$

Then we calculate combined shift and its error for the whole image as:

$$\sigma_{shift}^2 = \frac{1}{\sum_{k=1}^{stars} \frac{1}{\sigma_{shift,k}^2}}, \quad (4.6)$$

$$shift_{image} = \sigma_{shift}^2 \sum_{i=1}^{stars} \frac{shift_i}{\sigma_{shift,i}^2}. \quad (4.7)$$

Calculation of resulting magnitude is done by methods `get_shifted_light_curve()` of Sky-Object class in a similar manner as shift is calculated from catalogue magnitude as follows:

$$m_{object,image} = m_{object,image} + shift_{image}, \quad (4.8)$$

and error as:

$$\sigma_{m,object,image} = \sqrt{\sigma_{m,object}^2 + \sigma_{shift,image}^2}. \quad (4.9)$$

Transformation difference before and after applying this calibration can be seen in figure 4.3.

4.3.3 Photometry and Stacking

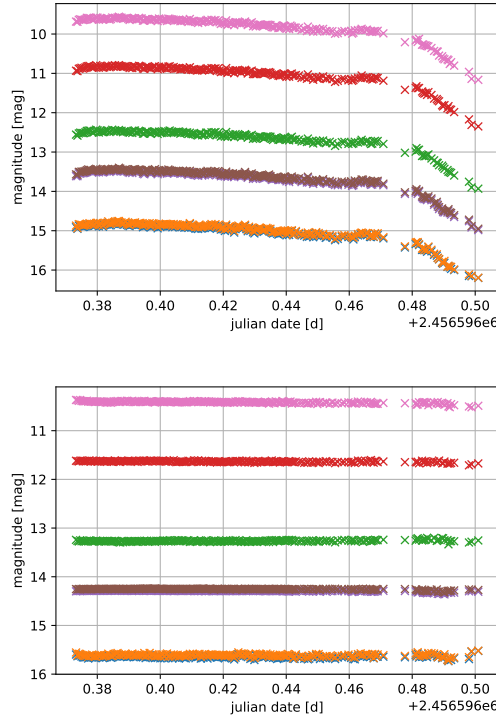
Since we are using procedures created by other authors that we incorporate in our package we wanted to test their behaviour whether it is according to our expectations when it comes to doing photometry and preserving flux when stacking images. To do so we proceeded with statistical tests on real data and compared it with our prediction.

Photometry

Photometry in our package can be described as follows: it firstly runs a method that converts sky coordinates of calibration stars/GRB to pixel locations in an image and this information is passed to a PythonPhot **aper** method along with image matrix and configuration. From what this method returns we recreate dictionaries containing resulting magnitudes and their errors and also save flux and sky value for GRB.

⁴average value of the pixels in an image

Figure 4.3: Before and after applying shift transform calibration. Image shows light curves for several calibration stars.



Stacking

The stacking procedure is a bit more complicated. We use images that have photometry done to have at least rough estimates of fluxes and magnitudes of GRB on input images. We created a manager that contains all necessary information to stack the images based on a parameter we chose to be a measure of signal to noise ratio (S/N); it can well describe how precisely we can calculate magnitude/brightness of an object. The very basic stacking is done using **ccdproc**, an astropy affiliated package, using its WCS reprojection and image combiner. We tested if the stacking procedure conserves the flux information and confirmed that difference between result and expected fluxes is smaller than associated errors.

The selection algorithm runs through the images and collects S/N for each. S/N is calculated as

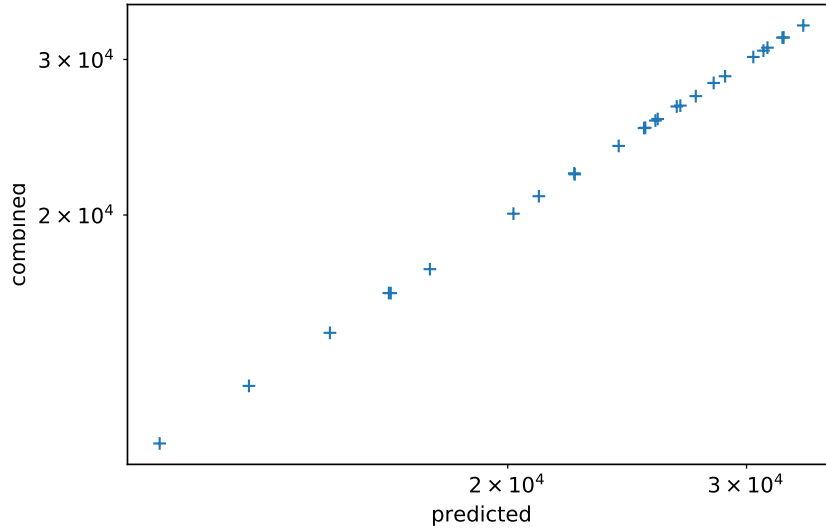
$$S/N = \frac{f}{\sigma_f} \quad (4.10)$$

If it finds image with S/N below given threshold it saves it and looks on the next image, collects its S/N, calculates predicted value of S/N of resulting image after stacking as

$$S/N_{pred} = \frac{\sum^i f_i}{\sqrt{\sum^i \sigma_i^2}}, \quad (4.11)$$

and compares this value again with the threshold. If the resulting S/N is of sufficient value it marks these images for stacking and continues with the same analysis for remaining

Figure 4.4: Plot of predicted vs. combined flux, it demonstrates consistent and correct prediction of flux. Fitting $\text{flux_predicted} = C \cdot \text{flux_real}^E$ gives us resulting parameters of $E = 0.9967 \pm 0.0031$ and $\log C = 0.0038 \pm 0.029$. Both E and C are compatible with 1, which proves correctness of our predictions.



images; if not it continues adding images until it meets the required S/N threshold or reaches end of image list. It is possible to experiment with the S/N threshold to get optimal stacking to get e.g. best fitting parameters for when later using the data. The formula for predicting the flux of resulting image made up of N images was:

$$f_{\text{predicted},N} = \frac{\sum^N f_i}{N}, \quad (4.12)$$

because the **ccdproc** image combining is done by averaging of input images. In the following tests we used stacking limit on S/N ratio for a GRB source of 4. This choice resulted in a different amounts of images to be stacked at different times. We then compare calibration stars which should remain of constant magnitude. The measured (raw) intensities of stars in our sample varied around 17-20 % (standard deviation) mainly due to atmospheric extinction which gave us range of fluxes to test the flux prediction for each star. Resulting image of plotted prediction vs. real combined flux is in figure 4.4.

We then split the images by median of flux for a star to observe spread of the differences between predicted and combined flux for predicting flux at lower flux values and higher flux values. Figure 4.5 demonstrates results based on which we can say there is no dependence.

Lastly we observed mean difference between predicted and measured flux. The ratio of the difference to average flux corresponds to the shift in magnitude; in figure 4.6 this value is show as it depends on absolute value of the flux.

Figure 4.5: Standard deviation of residuals normalized to Poissonian fluctuation; for each calibration star 3 points are drawn for the complete set of images, those with fluxes below median and above median respectively.

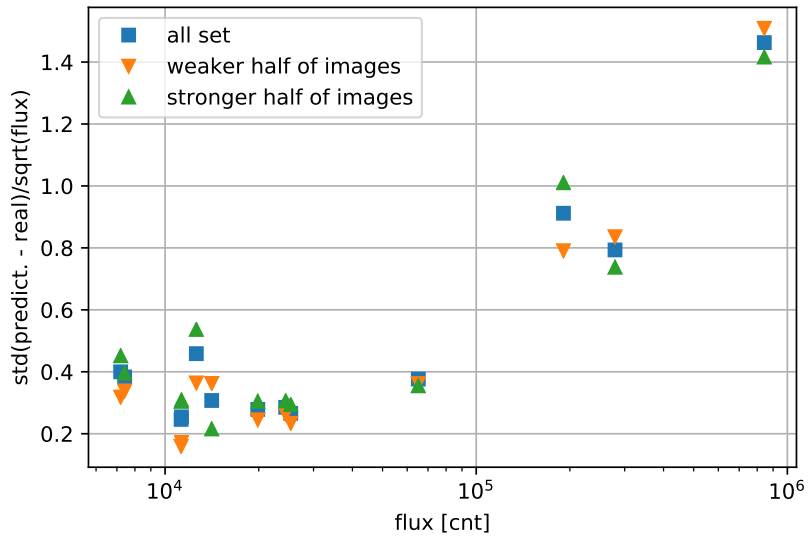
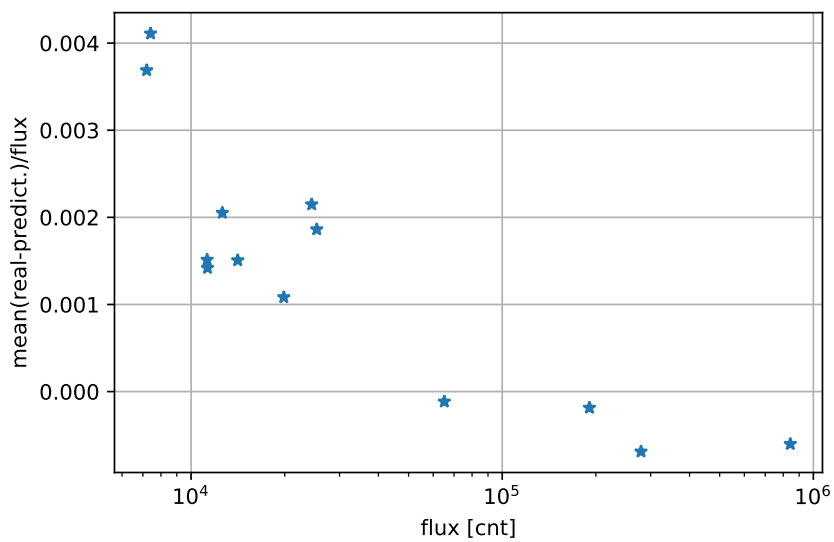


Figure 4.6: Relative average value of residuals for 13 calibration stars.



Chapter 5

GRB 131030A

In this chapter we show and discuss acquired data, our processed data and what available information was observed and acquired by other teams working with GRBs.

5.1 GCN information

The GRB 131030A was detected by Swift Burst Alert Telescope at 20:56:18 UT on October 30th of 2013 (GCN Circular #15042). The afterglow in X-ray and optical bands was identified by XRT and UVOT on board of the Swift satellite. Using UVOT observation the burst location was determined to be at $\alpha = 20^h00^m16.14^s$ and $\delta = -5^\circ22'5.2''$ with a $0.5''$ error radius at 90 % confidence level.(GCN Circular #15414). The BAT analysis determined T_{90} in 15 keV to 350 keV energy bands to be 41.1 ± 4 s. (GCN Circular #15456) There were two independent results for spectroscopy. First was done with 2.56 m Nordic Optical Telescope where a strong continuum was observed with features of Fe II, Mg II and Al II at redshift $z = 1.293$ identified as GRB, together with an intervening system with Fe II and Mg II features at $z = 1.16$ (GCN Circular #15407). The second spectroscopy was done with 10.4 m Gran Telescopio Canarias where there was strong trace of Al III, Zn II, Cr II, Ni II, Fe II at redshift $z=1.295$ identified as GRB, with an intervening system at $z=1.164$ (GRB Circular #15408). Konus-Wind observation found prompt emission and fitted time averaged spectrum at 20 keV to 15 MeV with Band function with peak energy E_{peak}^{obs} of 177 ± 10 keV, low energy photon index $\alpha = -0.71 \pm 0.12$ and high energy photon index $\beta = -2.95 \pm 0.28$ with $\chi^2 = 0.71$. Assuming previously mentioned redshift $z=1.293$ and standard cosmology model where $H_0=70 \text{ km s}^{-1} \text{ Mpc}^{-1}$, $\Omega_M=0.27$ and $\Omega_\lambda=0.73$, they estimated rest-frame parameters – isotropic energy release $E_{iso} = (3.0 \pm 0.2) 10^{53}$ erg, peak luminosity $L_{iso}=(1.0 \pm 0.1) \text{ erg s}^{-1}$, and rest-frame peak energy $E_{p,i}=(406 \pm 22) \text{ keV}$ (GCN Circular #15413). Early time polarized optical light curve with beginning at 655 s after burst for two hours uninterrupted, was observed with RoboPol instrument and preliminary analysis showed that source was linearly polarized at high significance (GCN Circular #15430); degree of polarization was later published in [25] to be $p=(2.1 \pm 1.6) \%$. Multiple optical confirmations of afterglow detection were present in GCN Circulars, most of these observations along with published values and filters used are summarized in table 5.2. [12]

Table 5.1: GRB 131030A GCN parameters

t_0	30.10.2013 20:56:18 UT
δ	$-5^{\circ}22'5.2''$
α	$20^h00^m16.14^s$
T_{90}	41.1 ± 4
z	1.293
E_{peak}^{obs}	177 ± 10 keV
α	-0.71 ± 0.12
β	-2.95 ± 0.28
E_{iso}	$(3.0 \pm 0.2) 10^{53}$ erg
L_{iso}	(1.0 ± 0.1) erg s^{-1}
$E_{p,i}$	(406 ± 22) keV

Figure 5.1: GCN observation data plotted.

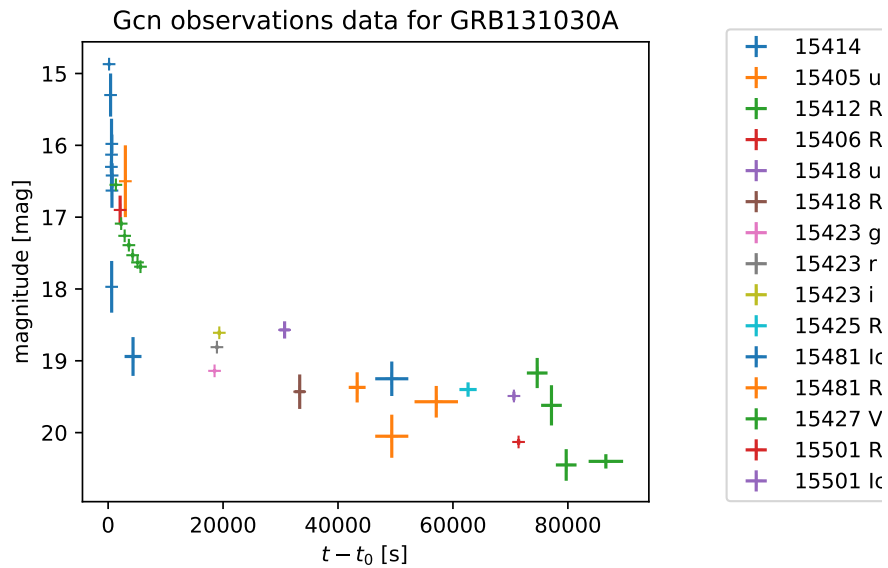
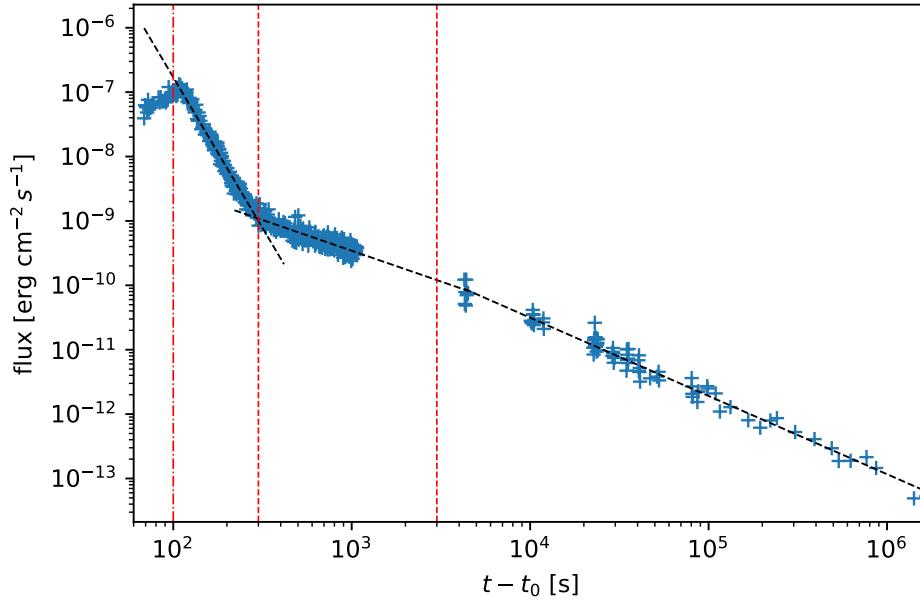


Table 5.2: Table containing optical observations of GRB 131030A shared in GRB Circulars also plotted in figure 5.1

$t - t_0$ [s]	exposure	magnitude	magnitude error	filter	GCN C#
164	148	14.87	0.02	w fc	15414
592	20	16.13	0.50	white	15414
427	246	15.30	0.30	u fc	15414
567	20	16.30	0.08	b	15414
641	19	15.98	0.13	v	15414
691	19	16.42	0.17	uvw1	15414
666	20	16.63	0.24	uvm2	15414
616	20	17.97	0.36	uvw2	15414
3000	180	16.50	3.50	unf	15405
1346	30	16.55	0.02	R	15412
2268	30	17.09	0.03	R	15412
2876	60	17.26	0.02	R	15412
3611	60	17.39	0.03	R	15412
4270	60	17.53	0.03	R	15412
5112	180	17.63	0.02	R	15412
5630	240	17.69	0.03	R	15412
86612	3000	20.40	0.10	R	15435
2088	0	16.90	0.20	R	15406
30708	900	18.57	0.12	unf	15418
33336	900	19.43	0.24	R	15418
18519	270	19.14	0.02	g	15423
18932	270	18.81	0.02	r	15423
19346	270	18.61	0.03	i	15423
62629	1500	19.40	0.10	R	15425
4334	1470	18.94	0.27	Ic	15481
49357	2880	19.25	0.24	Ic	15481
43334	1470	19.37	0.21	Rc	15481
49357	2880	20.05	0.30	Rc	15481
57097	3780	19.57	0.22	Rc	15481
74661	1800	19.17	0.21	V	15427
77144	1800	19.62	0.28	V	15427
79708	1800	20.45	0.22	V	15427
71421	300	20.13	0.04	Rc	15501

Figure 5.2: XRT data for GRB 131030A. Red dash dotted line indicates start of first region, each region is between two vertical lines, last being from the rightmost line to the end of data set. Black dashed lines are first fit models.



5.2 XRT data

For an afterglow in X-rays we used data available in Swift burst analyzer archive¹. We retrieved light curve with flux in energy range 0.3 – 10 keV. From first look at light curve it resembles a canonical X-ray afterglow as presented in [48]. We proceeded to fit the light curve with power-law decay

$$f = At^{-\alpha}, \quad (5.1)$$

in three different regions indicated on figure 5.2.

Results of the first fit show presence of a flare up until time $t - t_0 \sim 209$ s. We then moved adjusted start of the first region and refitted. With each resulting model for a region we calculated intersection of the power-law models and estimated break times. After several iterations resulting break times are

$$\begin{aligned} T_{break,1} &= 315 \text{ s}, \\ T_{break,2} &= 6678 \text{ s}. \end{aligned}$$

resulting fit can be seen in figure 5.3 and fit parameters in table 5.3. Parameter values are similar to those mentioned in [48] for a typical X-ray afterglow so our assumption was correct. We don't observe break at times on scales 10^4 to 10^5 s which should correspond to the position of an achromatic break.

¹http://www.swift.ac.uk/burst_analyser/00576238/

Figure 5.3: Resulting image with fit starting after X-ray flare (red dash dotted line). Red dashed lines indicate break times. Black dashed lines are fit models.

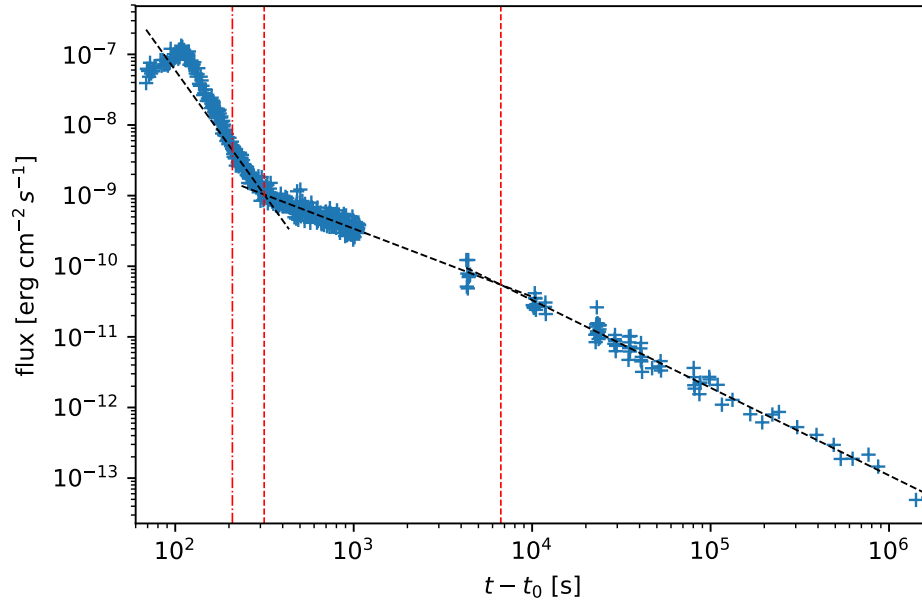
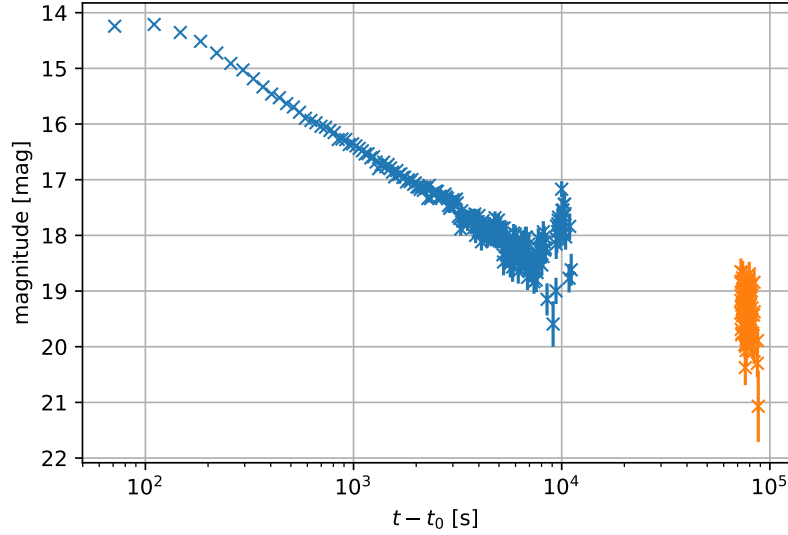


Table 5.3: Final temporal decay parameters from a power-law fit for GRB 131030A XRT light curve.

α_1	3.53 ± 0.11
α_2	0.96 ± 0.02
α_3	1.24 ± 0.2
$T_{break,1}$	315 s
$T_{break,2}$	6678 s

Figure 5.4: D50 optical data



5.3 D50 Optical data

Optical data were observed using D50 telescope and corrected, stacked (used limiting S/N ratio was 6) and analysed using GRBLC package. Resulting light curve used for further analysis is a combination of observations from two nights as shown in figure 5.4. We proceed fitting exponential decay as in the case of XRT, the times selected were for the seemingly flat part between times $t_1 \sim 150$ s and $t_2 \sim 4500$ s before the apparent brightening after t_2 . Residual plot (fig. 5.5) indicates presence of a break, which we calculated as intersection of two power-law fits to be at

$$T_{break} = 472 \text{ s},$$

using this parameter we used a model for broken power-law in form

$$f(t) = At^{-\alpha_1} T_{break}^{\alpha_1 - \alpha_2} + f_0, \quad (5.2)$$

$$f(t) = At^{-\alpha_2} + f_0, \quad (5.3)$$

for $t \leq T_{break}$ and $t > T_{break}$, respectively. Resulting parameters are shown in table 5.4. Model fit to both nights of observations is in figure 5.6 and residuals from the fit in figure 5.7. Next step was to determine the starting time of the brightness ‘‘bump’’, where we proceeded as described further in this section.

We didn’t find any features that would be similar for both optical and X-ray light curves.

Orthogonal regression fit for bump and ideal stacking S/N limit

Last we tried experimenting with orthogonal regression to find value of S/N that would be the best compromise between increased uncertainties in time and decreased uncertainties

Figure 5.5: residuals of initial power-law fit without break. Break estimate is indicate by dashed line.

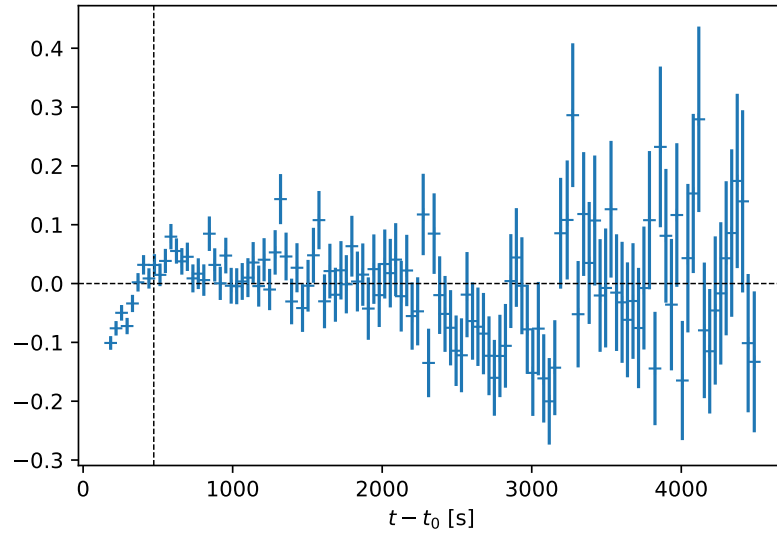


Table 5.4: Final temporal decay parameters from a broken power-law fit for GRB 131030A optical light curve.

α_1	1.20 ± 0.02
α_2	1.07 ± 0.01
$T_{break,1}$	472 s
f_0	145 ± 7

Figure 5.6: Fit of a model to data from both nights (blue points – first night, orange points – second night) accounting for the break, but excluding the “bump”. The red line model includes constant source of flux f_0 as opposed to the green line where $f_0 = 0$. Vertical dash dotted line indicates break time. Vertical dashed line indicates start of the “bump”.

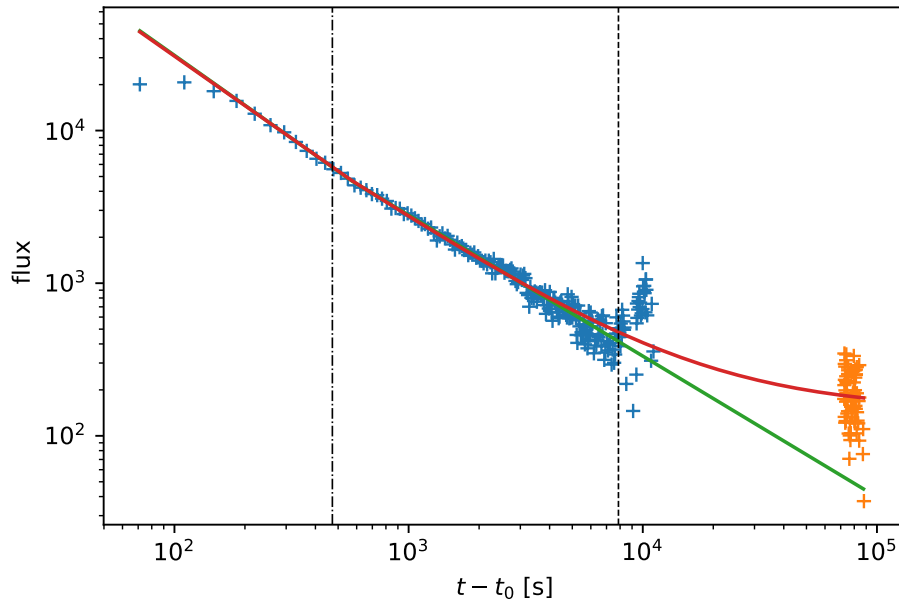


Figure 5.7: Residuals of final fit for optical data.

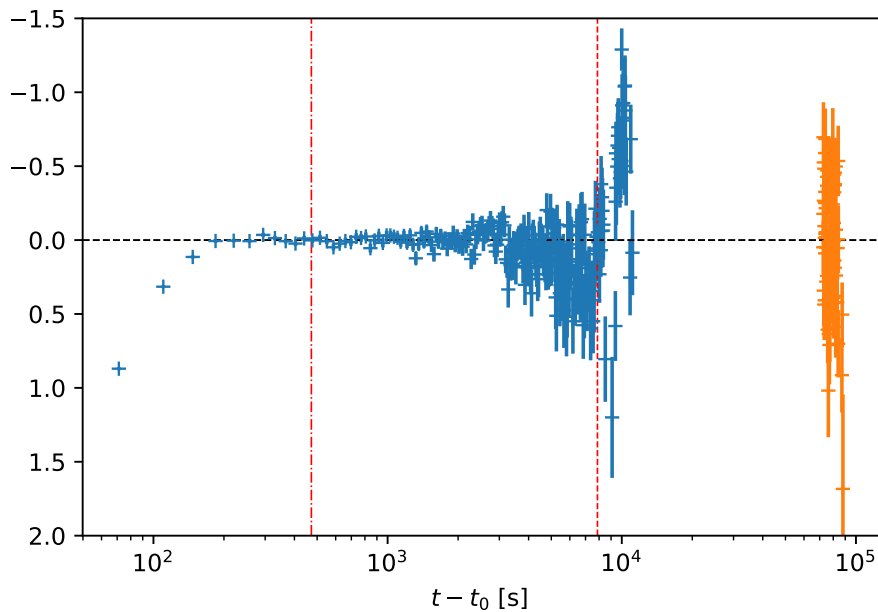


Table 5.5: Resulting bump times from orthogonal fits.

S/N limit	$T_{bump}[s]$	$\sigma_{T_{bump}}[s]$
no stacking	9182	101
2	9213	82
3	9258	81
4	9293	108
5	9316	105
8	9358	109

in magnitude. We tried to find the ideal stacking limit by fitting the light curve with a broken power-law described previously and the part of the bump by a line and determining the bump onset time as the intersection point of these curves. We created sets of images with different stacking limits and for each set determined times of bump along with their errors. We conclude that for finding the time of bump using orthogonal regression optimal S/N limit occurs for stacking between 2 and 3. Results of fit – times of break along with their errors are given in table 5.5, resulting fits plotted for each S/N ratio can be seen in figure 5.8 and 5.9.

Figure 5.8: Part 1 of plots of orthogonal fit to light curve and bump for different S/N stacking limitations. Black line is power-law model. Red line is line model for bump. Dashed vertical line is where first images had to be stacked. Width of the error band corresponds to 2σ distance from fitted line (after removal of outliers).

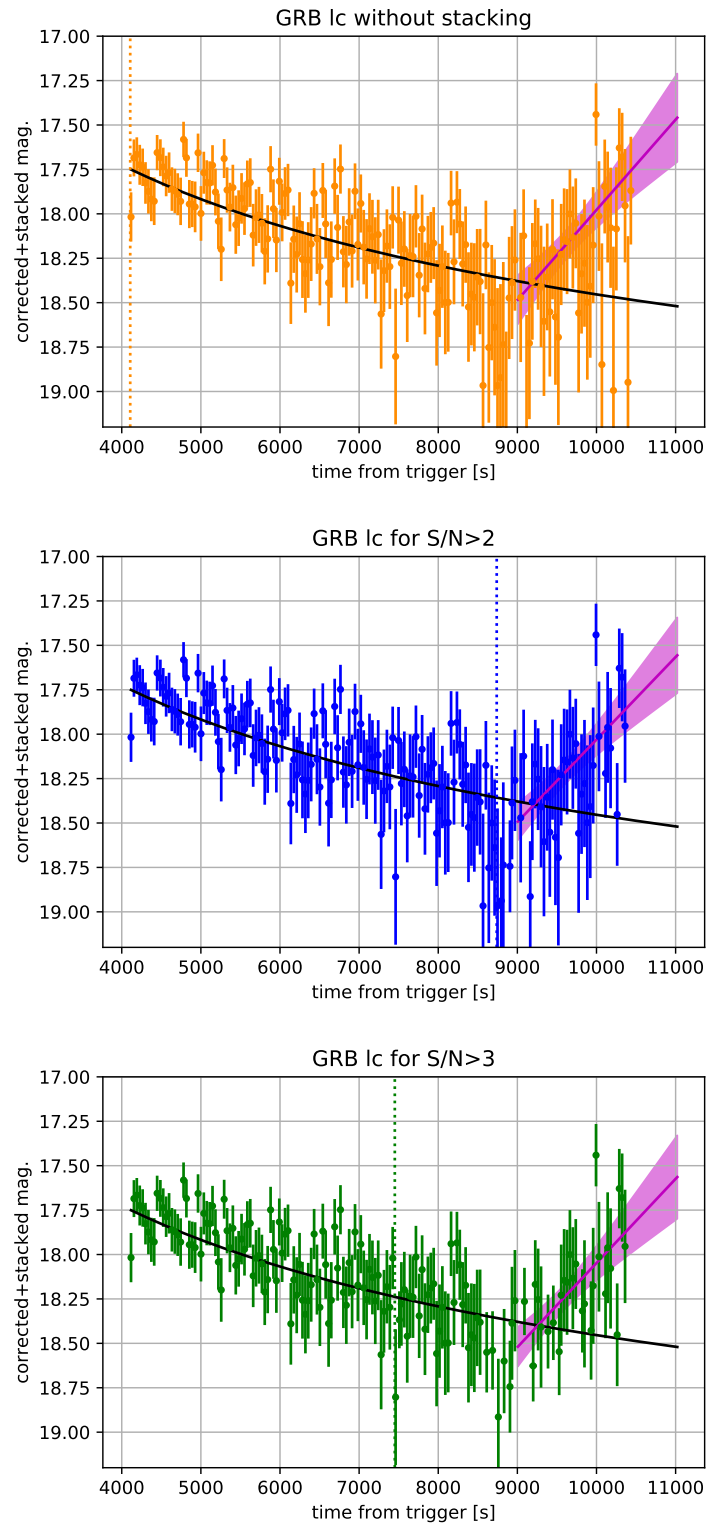
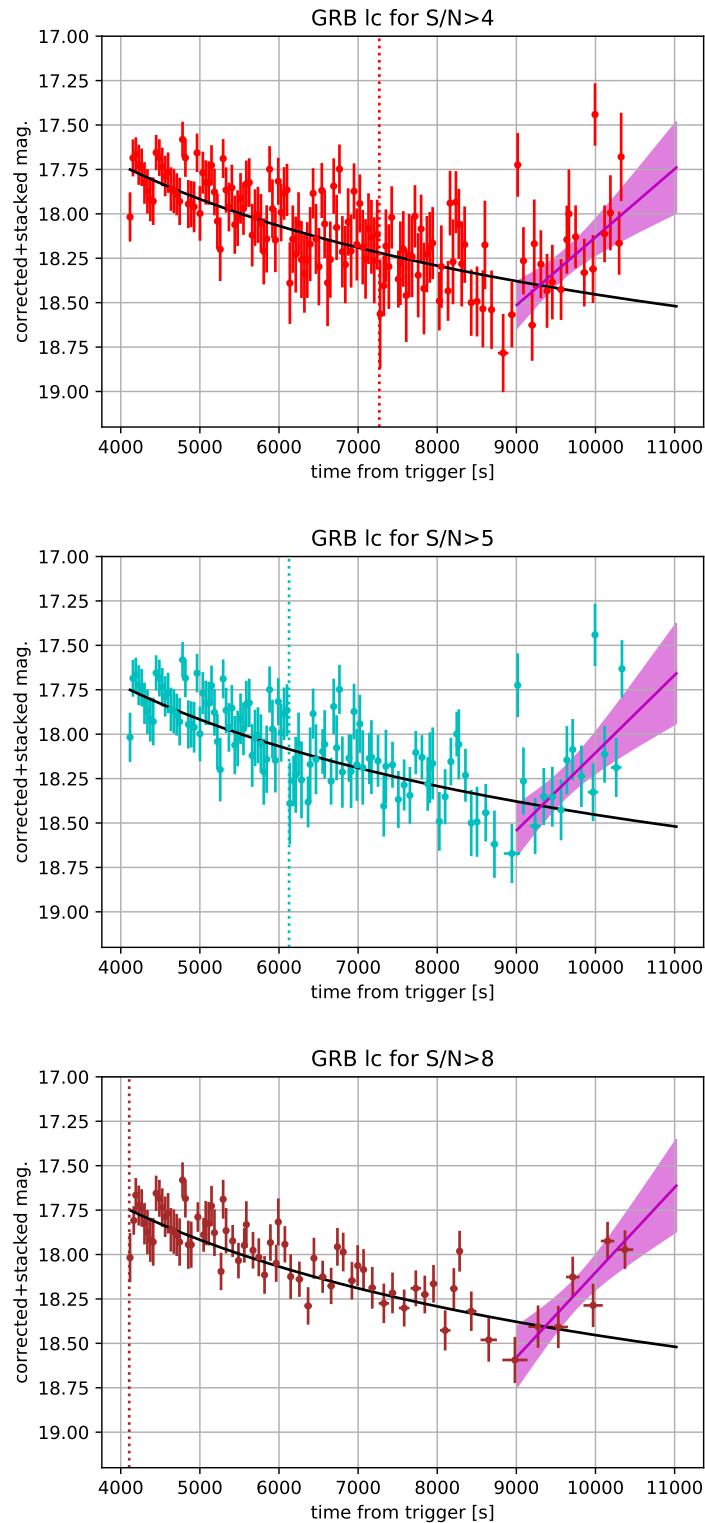


Figure 5.9: Part 2 of plots of orthogonal fit to light curve and bump for different S/N stacking limitations. Black line is power-law model. Red line is line model for bump. Dashed vertical line is where first images had to be stacked. Uncertainties of the exponential decay fit are too small to be resolved in the images.



Summary

In the first chapter we provided a brief overview on how GRBs were discovered and drew a simple timeline of events. In the second chapter we tried to outline basics of the most promising known model for GRBs and the physics behind it. In the third chapter we presented a GCN network that allows optical follow-up observations and helps sharing news in a GRB community. We also discussed a way of doing a CCD data reduction and demonstrated influence of atmosphere on ground based observations. In the fourth chapter we presented GRBLC package written in Python, that was created during this thesis, as a follow up after taking part in observations with a robotic telescopes at AI CAS Ondřejov. This code was designed with a thought of an easy expansion in the future; from programming point of view it is designed in a way that should allow this to happen. The concept is based on managers that take in transformers to process images in a certain way and allow another transformer to be applied later. The expansion can be done easily e.g. by adding more transformers for other purposes – be it automated light curve analysis or fitting. The package was created also with a secondary goal apart from its main functional purpose – to offer a clearly understandable code allowing for third party modifications for specific purposes. At the moment we have checked that the software is capable of processing observational data from D50 telescope but with no great effort it could be modified (if necessary) to process data from other ground based telescope that produce FITS image format outputs. We made a series of tests, results of which are described in second part of chapter 4, to confirm its usability and correctness. To our knowledge there is other already available software for processing CCD data however this package was made specifically for needs of processing a GRB optical observations and their calibration with a special emphasis on automated image stacking. Calibration is done using lists of stars in vicinity for which we query in online catalogues around the known GRB location. Automated selection of images depending on given signal to noise limitations of results is probably its unique feature. It allows to estimate the optimal limit of signal-to-noise for a specific purpose – be it fitting of a temporal decay or finding breaks in the light curve.

In the fifth chapter we presented available data for our selected burst – GRB 131030A. We demonstrated gathering information from GCN network that was described in chapter 2. We analysed light curve in X-ray band observed by XRT telescope aboard Swift. We concluded that it was a canonical X-ray light curve of a GRB afterglow with two breaks and a flare. We fitted the light curve with three separate models and found the times of breaks, determining temporal decay indexes for each section of the light curve. For optical data we proceeded in a similar way, after processing data with GRBLC we combined data from two observation nights and fitted the resulting optical light curve with temporal decay, found a break and a possible brightness “bump”. For the two differing parts of

light curve we determined the temporal decay indexes as well. We didn't observe any correlation between the light curves in X-ray and optical bands.

We believe this thesis can be a guide for anyone interested in using GRBLC and a source of information if he or she decides to expand it. In our opinion automation of analysis is the way to go in astronomy because the amount of data being created is significantly higher than the amount of data we are able to process. With that in mind we believe it is important to develop a system that would offer a physicist observed data in "humanly readable" form – for this reason we chose this direction instead of focusing on analysis of a single event.

Appendix

Example creating light curve with CCD data reduction using GRBLC.

```
from grblc.data_processing.datahandlers import FileHandler
from grblc.data_processing.datastructures import SkyObject
from grblc.data_processing.datahandlers import ObjectHandler, DatabaseHandler
from grblc.image_processing.stacking import StackingManager
from grblc.image_processing.transformators import *

darks_n1 = FileHandler("/home/foodiq/data/grbs/131030A/d50/c0/darks/",
                      query="*RA.fits",
                      data_type="dark").get_list()
flats_n1 = FileHandler("/home/foodiq/data/grbs/131030A/d50/c0/flats",
                      query="*RA.fits",
                      data_type="flat").get_list()
data_n1 = FileHandler("/home/foodiq/data/grbs/131030A/d50/c0/51018/",
                     query="*RA.fits",
                     data_type="data").get_list()

#create grb object
grb = SkyObject.grb(ra=345.06729,
                   dec=-5.3684,
                   trigger_jd=2456596.372431,
                   name="GRB131030A")
object_list = ObjectHandler(grb).get_list()

# prepare frames for correction
mdark_n1 = DarkTransform.create_master_dark(darks_n1, 20)
dark_n1_trans = TransformatorManager([DarkTransform(mdark_n1)])

flats_n1d = dark_n1_trans.apply_transformations(flats_n1)
mflat_n1d = FlatTransform.create_master_flat(flats_n1d)

# prepare transformators
phot_trans = PythonPhotometryTransform(object_list)
shift_trans = ShiftTransform(object_list)

transf_n1_compl = TransformatorManager([DarkTransform(mdark_n1),
                                       FlatTransform(mflat_n1d),
                                       phot_trans,
                                       shift_trans])

# apply all transforms
data_n1_corr = transf_n1_compl.apply_transformations(data_n1)
```

```
# unstacked results
grb.plot_light_curve(data_n1_corr,type="shifted", magerr=True)
#stacking
stack1 = StackingManager(data_n1_corr_filtered, grb)
stack1.select_images_to_stack(6)
stack1.plot_stack_prediction()
stack1.stack_images()

stacked_list_n1 = stack1.get_list()
# redoing photometry and calibration after stacking
phot_shift_trasnman = TransformatorManager([shift_trans,phot_trans])
stacked_list_n1_p = phot_shift_trasnman.apply_transformations(stacked_list_n1)
# saving results
db_n1 = DatabaseHandler("sqlite:///night1.db")
db_n1.save_objects_and_images(stacked_list_n1_p, object_list)
# plotting light curve
grb.plot_light_curve(data_n1_corr,type="shifted", magerr=True)
```

References

- [1] B. P. Abbott, R. Abbott, T. D. Abbott, F. Acernese, K. Ackley, C. Adams, T. Adams, P. Addesso, R. X. Adhikari, V. B. Adya, and et al. Gravitational Waves and Gamma-Rays from a Binary Neutron Star Merger: GW170817 and GRB 170817A. *ApJ*, 848:L13, October 2017.
- [2] C. Akerlof, R. Balsano, S. Barthelmy, J. Bloch, P. Butterworth, D. Casperson, T. Cline, S. Fletcher, F. Frontera, G. Gisler, J. Heise, J. Hills, R. Kehoe, B. Lee, S. Marshall, T. McKay, R. Miller, L. Piro, W. Priedhorsky, J. Szymanski, and J. Wren. Observation of contemporaneous optical radiation from a γ -ray burst. *Nature*, 398:400–402, April 1999.
- [3] L. Amati. The $E_{p,i}$ - E_{iso} correlation in gamma-ray bursts: updated observational status, re-analysis and main implications. *MNRAS*, 372:233–245, October 2006.
- [4] L. Amati, F. Frontera, M. Tavani, J. J. M. in't Zand, A. Antonelli, E. Costa, M. Feroci, C. Guidorzi, J. Heise, N. Masetti, E. Montanari, L. Nicastro, E. Palazzi, E. Pian, L. Piro, and P. Soffitta. Intrinsic spectra and energetics of BeppoSAX Gamma-Ray Bursts with known redshifts. *A&A*, 390:81–89, July 2002.
- [5] D. Band, J. Matteson, L. Ford, B. Schaefer, D. Palmer, B. Teegarden, T. Cline, M. Briggs, W. Paciesas, G. Pendleton, G. Fishman, C. Kouveliotou, C. Meegan, R. Wilson, and P. Lestrade. BATSE observations of gamma-ray burst spectra. I - Spectral diversity. *ApJ*, 413:281–292, August 1993.
- [6] N. Bucciantini, E. Quataert, J. Arons, B. D. Metzger, and T. A. Thompson. Relativistic jets and long-duration gamma-ray bursts from the birth of magnetars. *MNRAS*, 383:L25–L29, January 2008.
- [7] S. Campana, C. Guidorzi, G. Tagliaferri, G. Chincarini, A. Moretti, D. Rizzuto, and P. Romano. Are Swift gamma-ray bursts consistent with the Ghirlanda relation? *A&A*, 472:395–401, September 2007.
- [8] Zach Cano, Shan-Qin Wang, Zi-Gao Dai, and Xue-Feng Wu. The Observer's Guide to the Gamma-Ray Burst Supernova Connection. *Advances in Astronomy*, 2017:8929054, Jan 2017.
- [9] A. J. Castro-Tirado, F. M. Sánchez Moreno, C. J. Pérez del Pulgar, D. Azócar, G. Beskin, J. Cabello, R. Cedazo, L. Cuesta, R. Cunniffe, E. González, A. González-Rodríguez, J. Gorosabel, L. Hanlon, R. Hudec, M. Jakubek, P. Janeček, M. Jelínek,

- O. Lara-Gil, C. Linttot, M. C. López-Casado, M. Malaspina, L. Mankiewicz, E. Mau-reira, J. Maza, E. Muñoz-Fernández, L. Nicastro, E. O’Boyle, E. Palazzi, P. Páta, M. A. Pio, M. Prouza, F. Serena, M. Serra-Ricart, R. Simpson, P. Sprimont, J. Strobl, M. Topinka, S. Vitek, and A. F. Zarnecki. The GLObal Robotic telescopes Intel-ligent Array for e-science (GLORIA). In *Revista Mexicana de Astronomia y As-trofisica Conference Series*, volume 45 of *Revista Mexicana de Astronomia y As-trofisica*, vol. 27, pages 104–109, December 2014.
- [10] E. Costa, F. Frontera, J. Heise, M. Feroci, J. in’t Zand, F. Fiore, M. N. Cinti, D. Dal Fiume, L. Nicastro, M. Orlandini, E. Palazzi, M. Rapisarda#, G. Zavattini, R. Jager, A. Parmar, A. Owens, S. Molendi, G. Cusumano, M. C. Maccarone, S. Giarrusso, A. Coletta, L. A. Antonelli, P. Giommi, J. M. Muller, L. Piro, and R. C. Butler. Discovery of an X-ray afterglow associated with the γ -ray burst of 28 February 1997. *Nature*, 387:783–785, June 1997.
- [11] D. A. Frail, S. R. Kulkarni, L. Nicastro, M. Feroci, and G. B. Taylor. The radio afterglow from the γ -ray burst of 8 May 1997. *Nature*, 389:261–263, September 1997.
- [12] GCN Circulars GRB131030A. <https://gcn.gsfc.nasa.gov/other/131030A.gcn3>. [Online; accessed 1-May-2019].
- [13] Gcn. <https://gcn.gsfc.nasa.gov/>. [Online; accessed 1-May-2019].
- [14] Gcn. https://gcn.gsfc.nasa.gov/brief_describe.html. [Online; accessed 1-May-2019].
- [15] N. Gehrels, G. Chincarini, P. Giommi, K. O. Mason, J. A. Nousek, A. A. Wells, N. E. White, S. D. Barthelmy, D. N. Burrows, L. R. Cominsky, K. C. Hurley, F. E. Mar-shall, P. Mészáros, P. W. A. Roming, L. Angelini, L. M. Barbier, T. Belloni, S. Cam-pana, P. A. Caraveo, M. M. Chester, O. Citterio, T. L. Cline, M. S. Cropper, J. R. Cummings, A. J. Dean, E. D. Feigelson, E. E. Fenimore, D. A. Frail, A. S. Fruchter, G. P. Garmire, K. Gendreau, G. Ghisellini, J. Greiner, J. E. Hill, S. D. Hunsberger, H. A. Krimm, S. R. Kulkarni, P. Kumar, F. Lebrun, N. M. Lloyd-Ronning, C. B. Markwardt, B. J. Mattson, R. F. Mushotzky, J. P. Norris, J. Osborne, B. Paczynski, D. M. Palmer, H.-S. Park, A. M. Parsons, J. Paul, M. J. Rees, C. S. Reynolds, J. E. Rhoads, T. P. Sasseen, B. E. Schaefer, A. T. Short, A. P. Smale, I. A. Smith, L. Stella, G. Tagliaferri, T. Takahashi, M. Tashiro, L. K. Townsley, J. Tueller, M. J. L. Turner, M. Vietri, W. Voges, M. J. Ward, R. Willingale, F. M. Zerbi, and W. W. Zhang. The Swift Gamma-Ray Burst Mission. *ApJ*, 611:1005–1020, August 2004.
- [16] N. Gehrels, E. Chipman, and D. A. Kniffen. The Compton Gamma Ray Observatory. *A&AS*, 97:5–12, January 1993.
- [17] G. Ghirlanda, G. Ghisellini, and D. Lazzati. The Collimation-corrected Gamma-Ray Burst Energies Correlate with the Peak Energy of Their νF Spectrum. *ApJ*, 616:331–338, November 2004.

- [18] G. Ghirlanda, L. Nava, G. Ghisellini, and C. Firmani. Comments on “Are Swift Gamma-Ray Bursts consistent with the Ghirlanda relation?”, by Campana et al.(astro-ph/0703676). *arXiv e-prints*, April 2007.
- [19] J. Granot. Critical Review of Basic Afterglow Concepts. *arXiv e-prints*, November 2008.
- [20] F. A. Harrison, J. S. Bloom, D. A. Frail, R. Sari, S. R. Kulkarni, S. G. Djorgovski, T. Axelrod, J. Mould, B. P. Schmidt, M. H. Wieringa, R. M. Wark, R. Subrahmanyan, D. McConnell, P. J. McCarthy, B. E. Schaefer, R. G. McMahon, R. O. Markze, E. Firth, P. Soffitta, and L. Amati. Optical and Radio Observations of the Afterglow from GRB 990510: Evidence for a Jet. *ApJ*, 523:L121–L124, October 1999.
- [21] A. A. Henden, D. L. Welch, D. Terrell, and S. E. Levine. The AAVSO Photometric All-Sky Survey (APASS). In *American Astronomical Society Meeting Abstracts #214*, volume 214 of *American Astronomical Society Meeting Abstracts*, page 669, May 2009.
- [22] I. Horváth. A Third Class of Gamma-Ray Bursts? *ApJ*, 508:757–759, December 1998.
- [23] I. Horváth, L. G. Balázs, Z. Bagoly, F. Ryde, and A. Mészáros. A new definition of the intermediate group of gamma-ray bursts. *A&A*, 447:23–30, February 2006.
- [24] D. O. Jones, D. M. Scolnic, and S. A. Rodney. PythonPhot: Simple DAOPHOT-type photometry in Python. *Astrophysics Source Code Library*, January 2015.
- [25] O. G. King, D. Blinov, D. Giannios, I. Papadakis, E. Angelakis, M. Baloković, L. Fuhrmann, T. Hovatta, P. Khodade, S. Kiehlmann, N. Kylafis, A. Kus, I. Myserlis, D. Modi, G. Panopoulou, I. Papamastorakis, V. Pavlidou, B. Pazderska, E. Pazderski, T. J. Pearson, C. Rajarshi, A. N. Ramaprakash, A. C. S. Readhead, P. Reig, K. Tassis, and J. A. Zensus. Early-time polarized optical light curve of GRB 131030A. *MNRAS*, 445:L114–L118, November 2014.
- [26] R. W. Klebesadel, I. B. Strong, and R. A. Olson. Observations of Gamma-Ray Bursts of Cosmic Origin. In *Bulletin of the American Astronomical Society*, volume 5 of *BAAS*, page 322, June 1973.
- [27] C. Kouveliotou, C. A. Meegan, G. J. Fishman, N. P. Bhat, M. S. Briggs, T. M. Koshut, W. S. Paciesas, and G. N. Pendleton. Identification of two classes of gamma-ray bursts. *ApJ*, 413:L101–L104, August 1993.
- [28] W. H. Lee and E. Ramirez-Ruiz. The progenitors of short gamma-ray bursts. *New Journal of Physics*, 9:17, January 2007.
- [29] N. M. Lloyd and V. Petrosian. Synchrotron Radiation as the Source of Gamma-Ray Burst Spectra. *ApJ*, 543:722–732, November 2000.
- [30] M.S. Longair. *High Energy Astrophysics*. Cambridge University Press, 2011.

- [31] A. I. MacFadyen, S. E. Woosley, and A. Heger. Supernovae, Jets, and Collapsars. *ApJ*, 550:410–425, March 2001.
- [32] P. Mészáros. Gamma-Ray Bursts: Accumulating Afterglow Implications, Progenitor Clues, and Prospects. *Science*, 291:79–84, January 2001.
- [33] P. Mészáros. Gamma-ray bursts. *Reports on Progress in Physics*, 69:2259–2321, August 2006.
- [34] M. Nekola, R. Hudec, M. Jelínek, M. Kocka, P. Kubánek, F. Münz, C. Polášek, V. Šimon, and J. Štrobl. Robotic telescopes for high energy astrophysics in Ondřejov. *Experimental Astronomy*, 28:79–85, August 2010.
- [35] M. J. Rees and P. Meszaros. Relativistic fireballs - Energy conversion and time-scales. *MNRAS*, 258:41P–43P, September 1992.
- [36] M. J. Rees and P. Meszaros. Unsteady outflow models for cosmological gamma-ray bursts. *ApJ*, 430:L93–L96, August 1994.
- [37] Rts2 - remote telescope system 2nd version. <https://rts2.org/>.
- [38] K. C. Sahu, M. Livio, L. Petro, F. D. Macchetto, J. van Paradijs, C. Kouveliotou, G. J. Fishman, C. A. Meegan, P. J. Groot, and T. Galama. The optical counterpart to γ -ray burst GRB970228 observed using the Hubble Space Telescope. *Nature*, 387:476–478, May 1997.
- [39] R. Sari, T. Piran, and J. P. Halpern. Jets in Gamma-Ray Bursts. *ApJ*, 519:L17–L20, July 1999.
- [40] R. Sari, T. Piran, and R. Narayan. Spectra and Light Curves of Gamma-Ray Burst Afterglows. *ApJ*, 497:L17–L20, April 1998.
- [41] P. B. Stetson. DAOPHOT - A computer program for crowded-field stellar photometry. *PASP*, 99:191–222, March 1987.
- [42] Swift - discoveries. https://swift.gsfc.nasa.gov/about_swift/discoveries.html. [Online; accessed 27-April-2019].
- [43] Swift - info. https://swift.gsfc.nasa.gov/about_swift/. [Online; accessed 27-April-2019].
- [44] V. V. Usov. Millisecond pulsars with extremely strong magnetic fields as a cosmological source of gamma-ray bursts. *Nature*, 357:472–474, June 1992.
- [45] R. Vavrek, L. G. Balázs, A. Mészáros, I. Horváth, and Z. Bagoly. Testing the randomness in the sky-distribution of gamma-ray bursts. *MNRAS*, 391:1741–1748, December 2008.
- [46] S. E. Woosley. Gamma-ray bursts from stellar mass accretion disks around black holes. *ApJ*, 405:273–277, March 1993.

- [47] N. Zacharias, D. G. Monet, S. E. Levine, S. E. Urban, R. Gaume, and G. L. Wycoff. VizieR Online Data Catalog: NOMAD Catalog (Zacharias+ 2005). *VizieR Online Data Catalog*, 1297, November 2005.
- [48] Bing Zhang, Y. Z. Fan, Jaroslaw Dyks, Shiho Kobayashi, Peter Mészáros, David N. Burrows, John A. Nousek, and Neil Gehrels. Physical Processes Shaping Gamma-Ray Burst X-Ray Afterglow Light Curves: Theoretical Implications from the Swift X-Ray Telescope Observations. *ApJ*, 642(1):354–370, May 2006.

